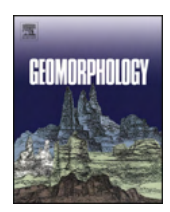


Contents lists available at ScienceDirect

Geomorphology

journal homepage: www.elsevier.com/locate/geomorph



Silica and iron mobilization, cave development and landscape evolution in iron formations in Brazil



Augusto S. Auler ^{a,*}, Hazel A. Barton ^{b,c,d}, Barbara Zambelli ^e, John Senko ^{b,c,d}, Ceth W. Parker ^f, Ira D. Sasowsky ^d, Tatiana A.R. Souza ^a, Diego Pujoni ^g, Jorge Peñaranda ^h, Reed Davis ^c

- ^a Instituto do Carste/Carste Ciência Ambiental, R. Barcelona 240/302, Belo Horizonte, MG, Brazil
- ^b Department of Biology, University of Akron, Akron, OH, United States
- ^c Integrated Bioscience, University of Akron, Akron, OH, United States
- ^d Department of Geosciences, University of Akron, Akron, OH, United States
- e Rua Espírito Santo 980/802, Belo Horizonte, MG, Brazil
- f Planetary Protection Center of Excellence, NASA Jet Propulsion Laboratory, Pasadena, CA, United States
- g Laboratório de Limnologia, Ecotoxicologia e Ecologia Aquática, Universidade Federal de Minas Gerais, Belo Horizonte, MG, Brazil
- ^h CEPAS, University of São Paulo, São Paulo, SP, Brazil

ARTICLE INFO

Article history: Received 31 August 2021 Received in revised form 1 December 2021 Accepted 1 December 2021 Available online 6 December 2021

Keywords: Iron formations Landscape evolution Speleogenesis Iron caves Iron porosity Iron reduction

ABSTRACT

Iron formations display some of the oldest and most enigmatic landforms on Earth, presently restricted to few areas of the planet. The original rock, the Banded Iron Formation (BIF) was formed in the Proterozoic and has been continuously weathered through a complex interplay of chemical and biological processes involving the massive mobilization of the main elements silica and iron, resulting in silica depleted (but friable) high-grade iron bodies and a Fe-rich surficial duricrust known as canga. This study presents new data and includes a comprehensive review of the existing literature, incorporating extensive data from unpublished reports and new findings. It aims to quantitatively analyze the morphology and development of porosity in iron formations both at micro and macro scales, assessing the geobiological mechanisms responsible for iron and silica mobilization and their role in the dynamics of this ever-evolving landscape. Silica leaching is the initial process of porosity generation at depth in the phreatic zone and results in a productive aquifer that contributes to the removal of solute and the generation of initial low-density zones. The development of numerous pores and voids is favored by the permeability contrast at the shallow contact zone between the canga and the weathered ore. Caves tend to occur at the base of scarps at the limit of plateaus and ridges, and tend to scale down in size away from the borders. The landscape evolves through the retreat of scarps, mostly through the collapse of cave passages. Caves exhibit a characteristic morphology that intercalates larger rooms and smaller connecting passages, suggesting that macropores started initially as isolated voids and occur either entirely in canga or in the weathered BIF, but commonly are associated with the contact between these rocks. Caves in the Amazonian Carajás region display the largest dimensional values, regardless of bedrock context. Longer caves show a larger number of connections between rooms, suggesting that the coalescence of rooms mostly through slope interflow processes is a key player in fostering the development of caves. Fractal Dimension (FD) calculated for the larger caves demonstrates that there is no relationship between lithology and FD, although values of FD vary between regions, with Carajás displaying the highest ones.

Geomicrobiological processes play a major role in the mobilization of iron through Fe(III) reducing bacteria. In particular, it promotes the long-term stabilization of voids through the generation of a hardened surface that protects the walls of caves and voids from collapse. The interplay of chemical and bacterial processes allows for the generation of a highly integrated network of pores and caves that represent outlets for the removal of silica and mobilization/concentration of iron. These voids are the result of geochemical leaching and evolve synchronously with the landscape, mostly at scarp level. Such processes connect isolated pores, promote evacuation of solutes and allow for the slow lateral degradation of the landscape. This geologically slow process is now heavily affected by mining operations, which reinforces the need for searching for mitigation and/or regeneration pathways in order to preserve this unique geo-biological ancient landscape.

© 2021 Elsevier B.V. All rights reserved.

^{*} Corresponding author.

E-mail address: aauler@gmail.com (A.S. Auler).

Contents

1.	Introduction									
2.	Geolog	gy, landforms and environment of if regions in Brazil	3							
	2.1.	Carajás	3							
	2.2.	Iron Quadrangle (IQ)	3							
	2.3.	Southern Espinhaço Range (SE)	4							
	2.4.	Weathering profiles and canga								
3.	Metho	ds	5							
4.	Geolog	gical and physiographical control. $\dots \dots \dots$	6							
	4.1.	Microporosity characterization	6							
	4.2.	Cave-landscape relationship	7							
	4.3.	Geological controls on cave dimension	8							
5.	Morph	nology of if caves	9							
	5.1.	Fractal Dimension								
		5.1.1. Lithological, geographical and morphological controls on FD	1							
	5.2.	Underground landforms and sedimentation	2							
6.	Genera	ation of porosity and speleogenesis	3							
	6.1.	Initial porosity	3							
	6.2.	Cave evolution	7							
7.	Iron m	obilization and landscape evolution	9							
8.		isions								
	Declaration of competing interest									
	Acknowledgements									
	Appendix A. Supplementary data									
Refe	References									

1. Introduction

Landscapes in iron formations represent some of the oldest land-forms and longest exposed rocks on Earth (Vasconcelos et al., 2019). The formation of massive iron deposits took place mostly during the Archean, with the largest volumes being precipitated between 3.5 and 2.5 Ga (Klein, 2005). Presently, iron formation regions occur in most climatic settings, with major deposits in Brazil, Australia, the Soviet Union, Canada and eastern/southern Africa (Bekker et al., 2010). Of note is the frequent occurrence of an iron-rich duricrust known as canga, which blankets the landscape, behaving as a protective cover that inhibits denudation and preserves, for long periods, the mostly friable subjacent iron formation bedrock. The peculiar geochemistry of these iron-rich environments results in very long surface exposure ages and low erosional rates (Monteiro et al., 2018a, 2018b) and thus these landforms usually stand as high elevation ridges and plateaus capped by canga.

Iron formations (IF) are here defined following Klein (2005), as a broad term that denotes not only the original rock, the Banded Iron Formation (BIF), but also a complex suite of weathering byproducts which result from various diachronic and long-lasting phases of BIF weathering. The initial stage involves silica/carbonate-removal, which may preserve the original rock banding, moving gradually towards a friable and porous rock due to extensive supergene and hypogene alteration processes (Rosière and Stacey, 2018). These weathered profiles can be as thick as 600 m (Rosière and Stacey, 2018) but are normally in the range of 50-100 m deep (Ribeiro, 2003). Their development involves iron mobilization and commonly the concentration of iron oxyhydroxides, resulting in high grade hematite ore deposits (>66% Fe; Dorr, 1965). The enigmatic canga cap is a later iron-rich conglomerate and various genetic interpretations have been proposed (Simmons, 1960; Dorr, 1964; Spier et al., 2019). Recently, it has been demonstrated that canga evolves through a "self-healing" mechanism (Monteiro et al., 2018a), in which iron mobilization and precipitation take place continuously, resulting in a dynamically regenerated crust that protects the friable subjacent IF.

The existence of pores and caves in IFs has been noticed since the 19th century (Pissis, 1849; Henwood, 1871) and numerous studies (*e.g.* Dixey, 1920; Axelrod et al., 1952; Campana et al., 1964; Marescaux, 1973; Bowden, 1980; Twidale et al., 1985) have later

commented on these features throughout the world, although detailed studies did not start until Simmons' (1963) research in Brazil. Caves, being underground features, allow for unique access to key geological features, which otherwise would tend to be masked by soil or largely obliterated by weathering at the surface (Plotnick et al., 2015). In the mostly flat canga-capped surface of IF regions, where canga limits the occurrence of outcrops of subjacent rocks, caves allow for a three-dimensional perspective of stratigraphic relationships that is largely unavailable at the surface. Furthermore, caves represent the macro dimensional analogue of small-scale (micro) porosity, and as such provide a window into a vast interstitial habitat characterized by highly heterogeneous pores and vugs, in which a complex interplay of chemical and bacterial processes take place (Levett et al., 2016; Parker et al., 2013b, 2018; Gagen et al., 2019b).

Besides their unequivocal economic and geomorphological importance, IF ecosystems are home to a unique faunal and floral biodiversity (Jacobi et al., 2007). Canga is a highly porous rock that hosts a diverse sub-surface habitat colonized by fauna adapted to this subterranean environment (Ferreira et al., 2015; Auler et al., 2019; Trevelin et al., 2019). The cave-adapted fauna in iron landscapes is more biodiverse than found in other rock types (Silva et al., 2011), and also comprise a remarkably rich microbiological community (Gagen et al., 2018; Parker et al., 2018; Calapa et al., 2021; Lemes et al., 2021). This porous environment includes also humanly accessible voids, here defined as caves. Thousands of caves have been recorded within and under the canga, representing an as yet little known speleological geo-ecosystem (Piló et al., 2015). Surface ecosystems are represented by endemic plants especially adapted to tolerate a high metal content environment (Skirycz et al., 2014; Schaefer et al., 2016; Jacobi et al., 2007, 2015; Zappi et al., 2019). These ecosystems display higher species richness when compared with areas of similar dimensions in other rock types (Gomes et al., 2019). They also host numerous archaeological and paleontological sites (Jacobi et al., 2015; Bittencourt et al., 2015) and have outstanding geoheritage value, comprising geographical landmarks as peaks, historical mining sites and early colonization structures (Ruchkys and Machado, 2013; Jacobi et al., 2015). Despite such unequivocal importance, iron-rich surface and subsurface environments are currently among the most threatened ecosystems in Brazil (Jacobi et al., 2015).

The commodity global market has seen a marked increase in iron prices since the late 2000's and presently most of the IF rocks are economically classified as "ore". In Brazil and elsewhere this has resulted in a dramatic increase in mining activities. The two largest IF regions in Brazil, Iron Quadrangle (IQ) in southeastern Brazil and Carajás in Amazonia, have been subject to major impacts to canga ecosystems. The IQ has witnessed a significant loss of canga areas, estimated at 50% (Salles et al., 2019) while Carajás has lost approximately 20% of its canga areas since 1973 (Souza-Filho et al., 2019). The remaining non-mined areas are largely either owned by mining companies or included in future mining plans (Jacobi et al., 2015). Although large patches of iron outcrops are essential for maintaining plant diversity (Salles et al., 2019), most preserved areas form disconnected and fragmented zones. Landscape and ecosystem degradation due to iron mining goes well beyond the immediate vicinity of open cast mines. It has been estimated that iron mining effects in the Carajás area may extend up to 70 km beyond mining lease boundaries and represents approximately 9% of all forest loss in the Amazon rainforest (Sonter et al., 2017). Considering the short life span of these mining operations (a few decades in most areas – Jacobi et al., 2015), post-mining scenarios hold the potential to be ecologically catastrophic.

There is, thus, a strong need for understanding and protecting this highly threatened environment. Studying the macroporosity of IF areas is crucial to setting up robust conservation and mining strategies (Nola and Bacellar, 2021). In Brazil, caves are protected by the constitution (Brasil, 1988), together with a protection buffer zone (Brasil, 1990; Auler and Piló, 2015). Due to the ubiquitous occurrence of caves in IF regions, this represents often the most straightforward way of protecting adjacent IF landscapes (Auler, 2016), even though up to 20% of these hypothetically protected buffer zones have been impacted in the IQ (Gomes et al., 2019). Environmental compensation related to caves has also resulted in the protection of significant IF areas at both the state and federal level, including the creation of new National Parks (Mota et al., 2018; Souza-Filho et al., 2019; Salles et al., 2019).

This research provides a review of the mechanisms of silica leaching and iron mobilization within IFs and the generation and development of porosity at both the micro and macro scale and how these processes affect the evolution of IF landscapes in the three most significant IF areas in Brazil, the Carajás area in northern Brazil, the Quadrilátero Ferrífero (Iron Quadrangle – IQ) and the Southern Espinhaco Range (SE) areas both in southeastern Brazil (Fig. 1). We have incorporated unpublished data about hundreds of caves, and provided an integrated model for their genesis, involving both geochemical and microbiological mechanisms. Our review also provides a link between IF porosity and the evolution of iron-rich plateaus in Brazil, which are directly connected with the evolution of high grade iron ore. The three study areas constitute over 90% of the iron production in Brazil (ANM, 2020) and are home of 2979 IF caves, approximately 95% of the total number of IF caves recorded in Brazil's official database (CANIE, 2021). A better understanding of these processes is important not only for conservation and management purposes, but also for providing insights on the dynamics of iron mobilization and enrichment that generates high-grade iron deposits.

2. Geology, landforms and environment of if regions in Brazil

The three major IF regions in Brazil (Fig. 1), Carajás, Iron Quadrangle (IQ), and Southern Espinhaço Range (SE), display canga deposits lying over friable altered IFs and are the focus of this work. Environmental studies for iron mine expansion have led to the identification of thousands of caves and catalyzed research on the genetic relationship between canga, weathered BIF and associated porosity. Although sharing geological similarities, these areas are presently located under distinct climate regimes, which result in marked surface and subsurface geomorphic and ecological differences.

2.1. Carajás

The giant Carajás iron deposit is in the Equatorial Amazon Rainforest biome. It comprises a Neoarchean metavolcanosedimentary sequence, mainly composed of BIF represented by jaspilites belonging to Carajás Formation of the Grão Pará Group, with a minimum age of 2.7 Ga (Trendall et al., 1998). This sequence lies unconformably over gneisses and granitoids of the Xingu Complex. The iron formations are covered by mafic rocks of Parauapebas Formation. The jaspilites show an intercalation of light and dark bands of iron oxide and silica (jasper and chert) of millimetric to centimetric thickness alternating with minor dolomitic rocks and irregular mafic rock intrusions (Lobato et al., 2005). The thickness of this sequence is up to 400 m (Klein and Ladeira, 2002). As a result of hydrothermal and weathering processes, the iron content of jaspillite is locally increased to over 64% (Lobato et al., 2005), forming the iron ore deposits. The most prominent structure in the area is the Carajás transcurrent fault, running in the E-W direction, which divides the iron deposits into North and South ridges (Serra Norte and Serra Sul) (Pinheiro, 1997) besides nearby East Ridge (Serra Leste) (Fig. 1B).

Climate in the Carajás region is of the Aw type in the Köppen classification, with an annual mean rainfall of ~2000 mm (Alvares et al., 2014), with 80% occurring between December and May (Silva Junior et al., 2017). Mean annual temperatures are approximately 26 °C (Alvares et al., 2014). The rupestrian vegetation over the canga plateaus comprises metal tolerant species adapted to restrictive edaphic conditions (Schaefer et al., 2016). The canga is bordered by dense Amazonian rainforest growing over iron scree and soils derived mostly from the igneous rocks. The Carajás region comprises a series of canga-capped plateaus of various sizes and shapes. Canga also occurs at the lower slopes, sometimes associated with fluvial valleys. The low relief top of the plateaus shows undulating surfaces and a few lakes filling depressions alike shallow dolines. The original area of canga-capped surfaces in Carajás was 144 km² in 1973, prior to the beginning of mining operations (Souza-Filho et al., 2019).

2.2. Iron Quadrangle (IQ)

The iron deposits of the IO, located in the mountainous highlands of southeastern Brazil, have been subject to scientific studies since the 19th Century (Eschwege, 1822) which detailed the stratigraphy (Derby, 1910; Dorr, 1969) and provided the first insights on the geomorphology of IF (Dorr, 1964, 1965, 1969). The area is characterized by a complex geological and tectonic evolution that involved hypogene and supergene iron mobilization (Rosière et al., 2018) and presently displays a series of ridges formed by the more resistant IFs (Fig. 1D). The iron-rich beds belong to the Cauê Formation and are locally known as itabirites. The BIF was deposited between 2.52 and 2.42 Ga (Babinski et al., 1995) and comprises interbedded quartz and hematite bands (with occasional carbonate), but also dolomite, magnetite, amphibole and lenses of marble and phyllite (Dorr, 1969). The thickness of the iron formation is highly variable, originally reaching approximately 250–300 m (Spier et al., 2006) but now may be as much as 1400 m due to tectonic processes (Dorr, 1964).

Climate in the IQ is humid subtropical, Cwa to Cwb according to Köppen and mean annual rainfall ranges between 1300 and 1600 mm (Alvares et al., 2014) concentrated during the austral summer. Shrubdominated vegetation over IFs exhibits a floristic identity, with extremely high local and regional diversity (Carmo and Jacobi, 2016). Unlike Carajás, there is no sharp vegetational transition away from the canga-capped ridgetops, since early European colonization has removed much of the original forested cover. Besides covering the ridge tops, IFs also occur in lower and less steep flanks. Anthropogenic impacts (mining, groundwater exploitation, agriculture, urbanization and deforestation) have profoundly altered the IQ landscape. The original exposure of IFs in the 1960's in the IQ was 186.4 km² (Salles et al., 2019).

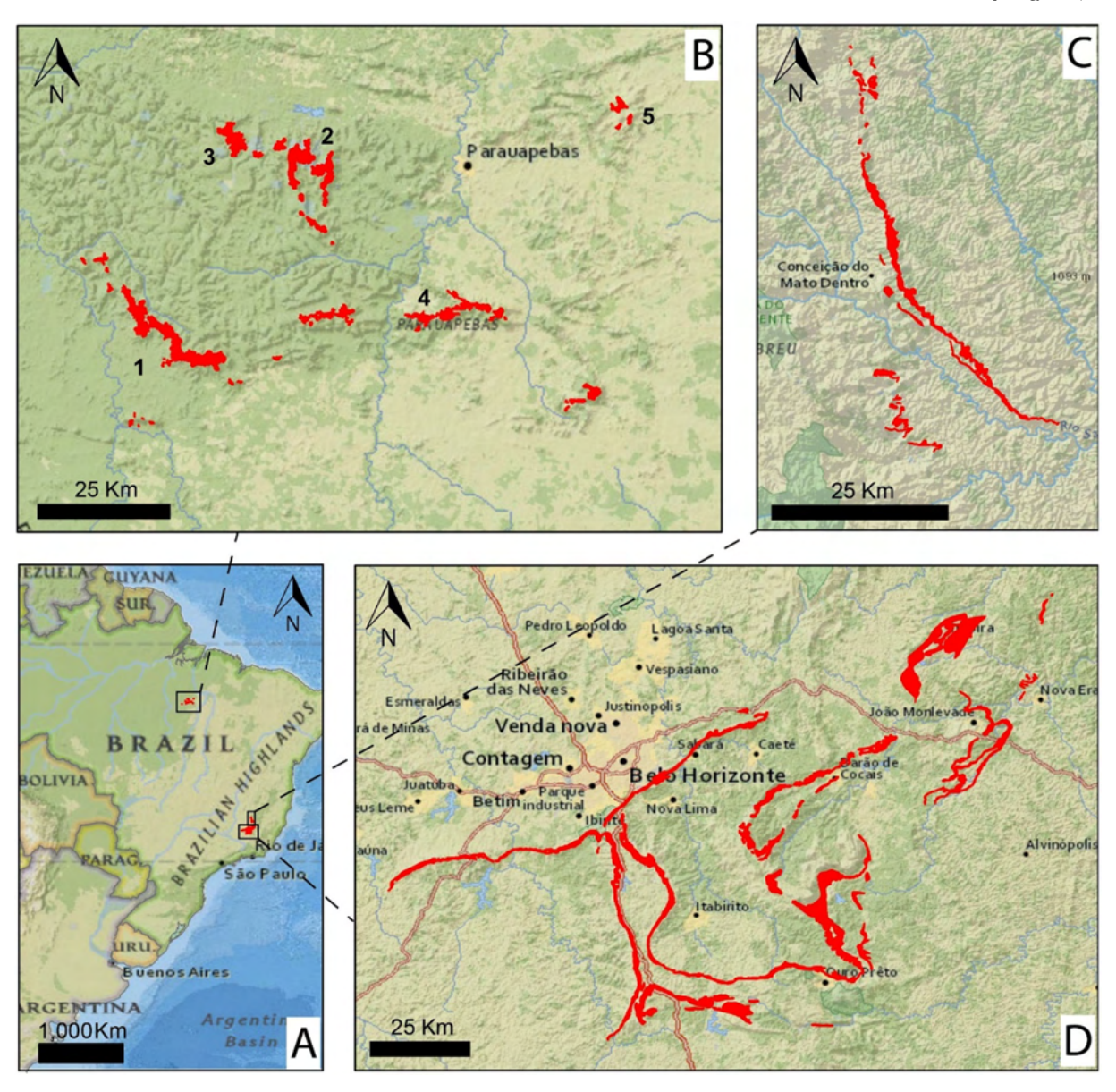


Fig. 1. (A) Location of the three study areas (IF outcrops in red) and sites mentioned in the text. (B) Carajás; (C) Southern Espinhaço and (D) Iron Quadrangle. Key for Carajás: 1. South Ridge; 2. North Ridge; 3. N1 (a plateau that belongs to North Ridge); 4. Bocaina plateau (part of South Ridge); 5. East Ridge.

2.3. Southern Espinhaço Range (SE)

The Southern Espinhaço Range IFs (Fig. 1C) are located close to the IQ, and thus share many of the same climatic and vegetational characteristics. The Fe-rich deposits comprise two distinct sequences separated by an erosional unconformity. They belong to the Serra do Sapo Formation of the Serra da Serpentina Group, and the Canjica Formation of the São José Group, with depositional ages respectively at 1.99 and 1.66 Ga (Rolim et al., 2016). Both BIF formations exhibit similar characteristics with mm to cm thick alternate hematite-rich and quartz-rich banding. The Serra do Sapo Formation has an average iron content of 32.5 wt%, but contains some higher grade ore bodies (Rolim et al., 2016). The thickness varies from a lower value of 15 m in the southernmost portions to up to 350 m in the northern sector (Rosière et al., 2018). As in the IO, the SE deposit outcrops mostly at the top and flanks of irregular roughly N-S trending ridges. Total area of iron outcrops, as estimated from Rolim et al. (2016) is 34.2 km². Cattle and dairy farming have altered the original vegetation. Iron mining operations in the SE started in the early 2010's, thus most of the IF deposits are still preserved.

2.4. Weathering profiles and canga

The IFs as exposed presently in all three regions are the result of massive long term weathering processes and groundwater-related leaching of constituents (Rosière et al., 2008; Rosière and Stacey, 2018). These processes have considerably modified the original BIF, resulting in a heterogeneous and non-coherent rock, colloquially termed "hard" and "soft" ores, which relates not only to its friability but also to whether it is dominantly hematite or goethite/other Fe-hydroxides (Rosière et al., 2008). Particularly in the IQ leaching of carbonates and silica are believed to have resulted in low density collapse-prone zones and the deepest weathering profiles (up to 400 m) tend to occur beneath the high grade iron bodies (Ribeiro et al., 2021). In Carajás the thickest weathering profiles are associated with the doline-like depressions occupied by lakes (Ribeiro, 2003).

Characteristic of all three areas (and elsewhere in Brazil and several IF areas in the world) is the occurrence of canga, an iron-rich duricrust that caps and protects the underlying friable rock from erosion. The overlying canga in average contains over 90% Fe₂O₃ and is composed of fragments inherited from the BIF, cemented by goethite, minor

gibbsite and rare manganese oxides and phosphates (Spier et al., 2019). Thickness varies from a few centimeters to more than 30 m, averaging 1-2 m (Dorr, 1964). Dorr (1964) realized that canga must be continually renewed, otherwise it would have been removed over geological time. This has been confirmed by ⁴⁰Ar/³⁹Ar and (U/Th)/He dating of canga in Carajás and IQ which has yielded stratigraphically noncoherent ages (Monteiro et al., 2014; Spier et al., 2006; Monteiro et al., 2018a, 2018b) showing that iron mobilization and reprecipitation has occurred over millions of years (Vasconcelos and Carmo, 2018; Levett et al., 2020a, 2020b, 2020c). Erosion rates in the weathering profiles are in the range of 0.20-0.24 m/Ma for Carajás (Monteiro et al., 2018b) and 0.17-0.31 m/Ma for three ridges in the IQ (Monteiro et al., 2018a), which represent extremely low values, over two orders of magnitude lower than the world's average based on drainage basins (Sasowsky, 2007), helping explain the geomorphic resilience of IF plateaus and ridges.

Several hypotheses have been proposed to explain the genesis of canga (see review in Simmons, 1960 and Dorr, 1964), involving *per ascensum* or downward/laterally water flowing processes; *in situ* hydration of hematite and partial leaching of quartz; replacement of former soil horizons, among others. The role of bacteria, first commented by Dorr (1964) in the IQ but also by McFarlane and Twidale (1987), has been confirmed by Parker et al. (2013a, 2013b) and Levett et al. (2016), showing that microbially mediated redox processes are an important catalyst of Fe mobilization and recycling. The presence of plant structures preserved within canga shows that vegetation can also significantly influence the evolution of canga (Gagen et al., 2019b; Paz et al., 2020). The complex, and still little known, interaction of biological and chemical processes is critical for the understanding of canga dynamics, high-grade ore preservation and landscape evolution in IF regions.

3. Methods

This review article made use of extensive data from consulting and mining companies, besides speleological studies made by professional and amateur caving clubs. The integration between these comprehensive archives of geological and speleological data allowed for insights on the genesis and relevance of caves to both the long term geomorphic evolution of IF regions and the generation of high grade ore.

Several 51 mm diameter, approximately 30 cm long, cores were drilled perpendicular to the surface in canga areas in both the IQ and SE areas using a Shaw portable core drill (www.backpackdrill.com), to allow for the measurement of permeability. A total of 24 cores were selected and cut both perpendicular and parallel to the surface. Permeability measurements were made with a TinyPerm air permeameter (http://www.ner.com/site/systems/item/27-tinyperm.html) from CEPAS, University of São Paulo. Five measurements were performed in each sample, totaling 125 measurements.

For our cave data set we have adopted Brazil's official definition of cave, an anthropocentric concept that restricts caves to natural voids enterable by humans (Palmer, 2007). A consensual 5 m minimum length has been applied for most consulting works in Brazil. Although this leaves a two order of magnitude gap between the pores analyzed through core drilling and the caves available for direct inspection, a dimensional continuum can be observed. We treat the larger caves as macro dimensional analogues resulting from the development of smaller voids. Such transition can be observed inside caves, which are subject to the same processes of iron mobilization.

The Brazilian National Cave Database (CANIE — https://www.icmbio.gov.br/cecav/canie.html) was used for obtaining general locational information about IF caves. Much of our analyses was based on speleological reports by the consulting company Carste Ciência Ambiental. These reports have been archived in the national or state environmental agencies and in public domain websites. Data from Carajás can also be accessed in Jaffé et al. (2016, 2018). Our data set comprised a total of 1155 caves in Carajás, 405 in the IQ and 271 in the SE (total of

1831 caves). This data set is restricted to caves developed entirely in IFs. Caves at the contact with other rock types (such as mafic rocks common in Carajás) were discarded as well as caves in Fe-rich soil classified as ferricrete. For each cave, besides a detailed survey map, general information about the dimensions (length, depth, area, volume), local geology, cave pattern, cave geological features were provided, allowing for a quantitative assessment of the relationship between these parameters. For cave morphometry we have defined a 50 m minimum length for extracting meaningful morphometric information, which resulted in 238 caves, being 185, 36 and 17 respectively in Carajás, IQ and SE.

Statistical analyses were performed using Microsoft Excel® and R software (v.3.6.1) (R Core Team., 2019). Relations between morphometric variables were quantified and tested by the calculation of Pearson correlation index. In addition, a linear regression was performed in order to model the relation between cave area and volume. Percentilic confidence intervals were calculated through a quantile regression.

Fractal analysis was applied to the 238 caves larger than 50 m. The aim was to investigate how the Fractal Dimension (FD) relates to the cave's morphology, lithology, size (length and area), and location. For this, the first step was to perform a 2D fractal investigation in order to calculate the Fractal Dimension. Caves were analyzed using two different software, ImageJ with FracLac plugin (https://imagej.nih.gov/ij/ plugins/fraclac/FLHelp/Introduction.htm), and Fractal Analysis 3.4.7 (http://cse.naro.affrc.go.jp/sasaki/index-e.html). Since this software only accepts binary and grayscale bitmap files as input, it was necessary to perform the conversion of all cave maps, originally in jpg or pdf format, to an 8-bit image (where white would represent the space inside the cave - voids - and black everything else - pillars, rocks, cave walls). This conversion was performed with Adobe Illustrator for vector images (pdf) and with Power Point and Paint for non-vector ones. The process consists in erasing details inside the caves such as drainage, speleothems, blocks and contours, and leaving only the external walls. If the cave has more than one level, its projected maximum extension was adopted. After the conversion, all the images were saved in the same size and resolution (512 \times 256 points, 150 dpi) for standardized analysis, since images with different formats, sizes or resolution would result in diverse Fractal Dimensions. An example of this output is shown in Fig. 2.

The software (ImageJ/FracLac and Fractal 3.4.7) use boxcounting (box sizes range from 2 to 1024 pixels) and further linear regression to calculate FD. For FracLac, the number of boxes was fixed, while for Fractal 3.4.7, the number of boxes varied from cave to cave and was not clear in the calculations. The number of boxes is important because it directly affects the FD calculation. After calculating FD, statistical analyses were performed using Microsoft Excel to verify possible correlations. The relationship involving cave length, area and FD were investigated by means of Pearson correlation.

We imaged the BIF, canga and cave wall samples using a Nikon XTH 320 CT system (Nikon Metrology Inc., Brighton, MI, USA), housed in the National Center for Education and Research on Corrosion and Materials Performance (NCERCAMP) at The University of Akron. Settings used for the scan can be found in Table 1. We reconstructed the CT images of each sample using NRecon (v.1.7.4.2, Bruker, Kontich, Belgium) by following the manufacturer's instructions to import a non-proprietary dataset and saved the output as 16-bit TIFF images to maintain the range of grey values in the images. Following reconstruction of the CT images, we loaded the images into DataViewer (v. 1.5.6.2, Bruker) to align the reconstructed sample vertically. This step ensures that pores are not measured obliquely during morphometry and provides more accurate data. Following alignment, we employed CTAnalyser (v. 1.19.11.1, Bruker) to crop a volume of interest (VOI) near the center of each sample. We did this to ensure equal sample size and to minimize the effects of artifacts near the edges of the samples. The final size of the VOI for each sample was 3.44 \times 2.67 \times 10.13 mm. Using these new VOIs of each sample, we gathered morphometric data of the rock and pore phases of the sample using built-in plugins of CTAnalyser.

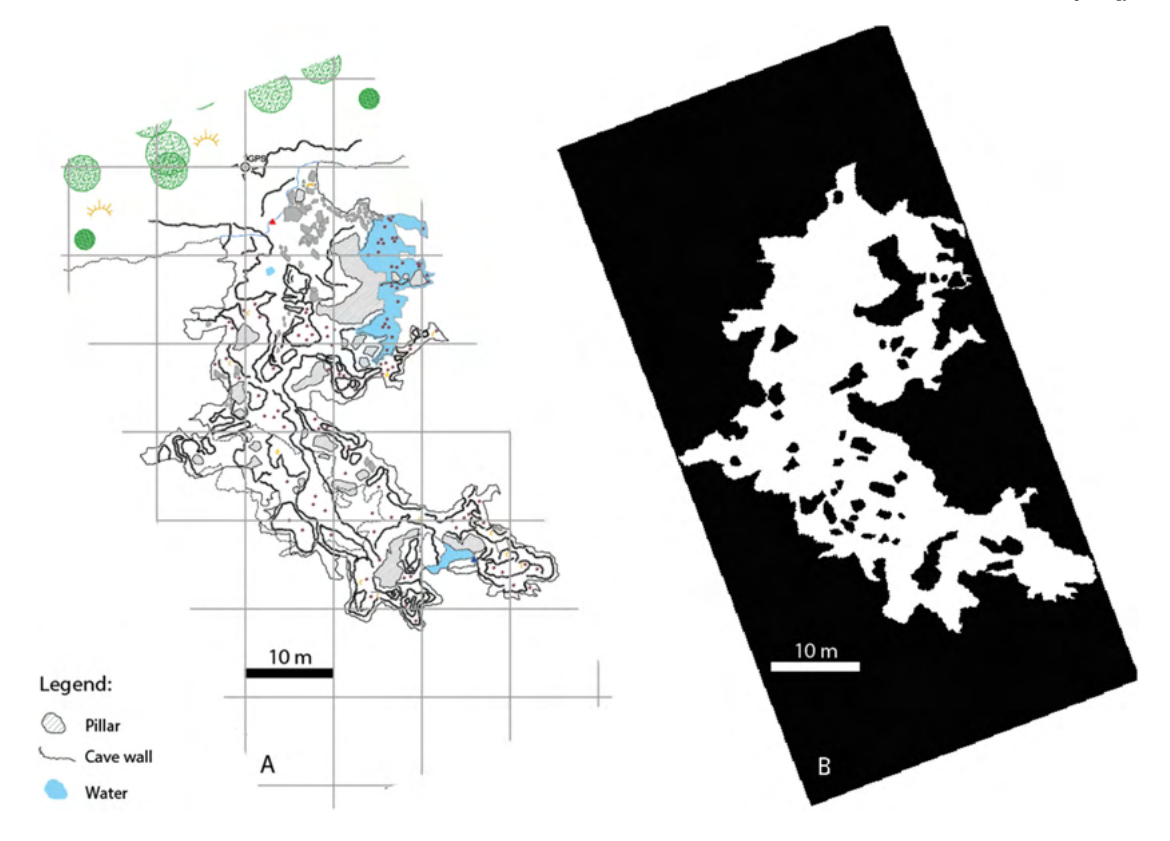


Fig. 2. (A) Original map (pdf format) of a cave. (B) 8-bit grayscale resulting image used to perform the fractal analysis.

These morphometric data included total volume (TV), rock volume (RV), percent rock volume (RV/TV), rock surface area (RS), rock surface to volume ratio (RS/RV), pore diameter (PD), pore separation (PS), number of closed pores (CP), volume of closed pores (CV), volume of open pores (OV), percent open pores (OV/TV), percent closed pores (CV/TV), and percent total porosity ([OV + CV] / TV, TP). The specific tasklist used was determined through extensive trial and error testing and can be found in the Suppl. Table 1. Three-dimensional (3D) renders of the rock and the pore systems were visualized using Dragonfly (v. 4.1.0.647, Object Research Systems, Montréal, Canada).

4. Geological and physiographical control

4.1. Microporosity characterization

The two types of BIF weathering products, canga and the friable bedrock underneath, are highly porous, but in distinct ways. Due to the mostly unconsolidated nature of the friable iron bedrock, porosity and aquifer storativity increases with degree of weathering, but permeability tends to decrease (Bertachini et al., 2018). Porosity values between 24 and 29% (Costa and Sá, 2018) and 14 and 24% (Dias and Bacellar, 2021) have been reported, depending on the type of canga and area. The friable ore behaves as a heterogeneous and anisotropic aquifer,

Table 1Scan parameters used for CT imaging.

Scan parameter	Scan setting
Source voltage	220 kV
Source current	240 μΑ
Filter	1.0 mm tin
Pixel size	15.98 μm
Rotation step	0.11°
Exposure	708 ms
Total sample rotation	360°

with flow being controlled by relict banding and foliation (Bertachini et al., 2018). Permeability values of 10^{-8} m/s have been reported (Mesquita et al., 2017), and values can be as much as three times higher along the banding (Mourão, 2007). The upper boundary of the friable ore is mostly at high elevations, entirely in the vadose zone, and normally does not store water, except temporarily during rainfall events.

Canga, being a later byproduct, does not display banding or foliation, although it is common to show irregular unloading joints (sensu Allaby, 2013) parallel to the surface. Canga is mostly impermeable at the surface (Dorr, 1964) but is highly porous, displaying large and irregular vugs that form a continuum towards larger caves and represent a habitat for subterranean adapted fauna (Auler et al., 2019). Our cores show the preferential concentration of vugs along specific horizons, probably controlled by redox fronts or perched water levels. Unloading also favors the expansion of surface-parallel voids. Permeability measurements in the IQ and SE (Supplementary Material Table 2) show a high degree of anisotropy (Fig. 3), with the largest values being along horizons with preferential concentration of vugs. Measurements perpendicular to these horizons were so low as to prevent obtaining meaningful data. Average values of hydraulic conductivity in the IQ $(8.00 \times 10^{-4} \text{ m/s})$, although in the same order of magnitude, are twice as large as in the SE (4.04×10^{-4}) . This may reflect local differences between drilling sites. Values between 2.31×10^{-6} and 2.80×10^{-4} have been reported for Carajás (Bertachini et al., 2018). The high permeability of canga is comparable to unconsolidated rocks such as gravel, highly fractured rocks or even karstified carbonate (Fig. 3), but unlike in those rocks, it is developed through the dynamic generation of vugs by chemical and biological processes.

The extreme permeability contrast between the highly porous canga and the less permeable lower friable ore results in the temporary storage of water in this contact zone (Bertachini et al., 2018). The hydraulic gradient tends to increase towards the borders of plateaus and ridges, and thus the horizon represented by the canga/ore contact is a focal point for water movement and solute removal.

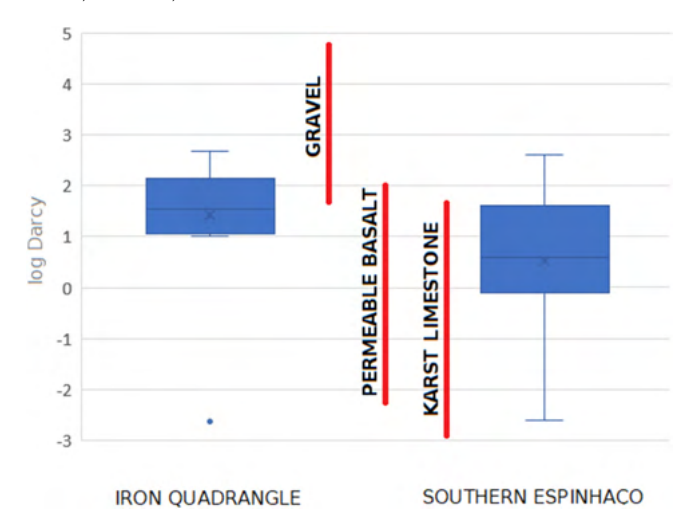


Fig. 3. Boxplot of hydraulic conductivity values obtained from 125 measurements in canga samples from the IQ (left) and SE (right). Values are highly heterogeneous as they reflect the concentration of vugs along specific horizons. For the complete set of values see Supplementary Material Table 2.

Range of values for other rock types based on Freeze and Cherry (1979).

4.2. Cave-landscape relationship

The canga cap that overlies the plateaus and ridges tends to be continuous, generating an undulating landscape with few protruding outcrops. In the IQ and SE the IFs are in contact with quartzites, a geochemically resistant rock that is also subject to very low (<3 m/Ma) denudational rates (Salgado et al., 2008). The quartzites help support the ridge topography typical of these areas. In Carajás, the canga plateaus are surrounded by igneous rocks, which weather quickly under the equatorial climate. This results in sharp changes in elevation (approximately 300 m) between plateau tops and the surrounding lowlands. In all three areas, the contact between the canga cover and the

surrounding rocks is marked by small scarps. IF scarps are ubiquitous landforms and represent sharp breaks in the topography (Figs. 4, 5B). Scarps are typically between 2 and 10 m high, run perpendicular to the slope, marking the ridge/plateau limit, are irregular both vertically and longitudinally and can extend laterally for several hundreds of meters. Scarps in Carajás tend to be more extensive and higher than in the other two areas. Scarps are undoubtedly among the most important geomorphological features of IF areas. They host the vast majority of IF caves, denoting a clear association between caves and plateau/ridge boundaries (Fig. 4). Generally, there are three situations in which caves are not associated with scarps: (i) when located at inner lake borders as in the South Ridge of Carajás; (ii) when located in the interior of plateaus and ridges, normally linked to the collapse of canga cave ceilings or associated with minor outcrops; (iii) when associated with fluvial valleys in the lower slopes. These alternative locations tend not to include the larger and more representative caves.

Scarps are also important because they represent the dynamic boundary of plateaus and ridges (Vasconcelos and Carmo, 2018; Vasconcelos et al., 2019) since the landscape evolves, albeit very slowly, through scarp disintegration and retreat. Scarps commonly mark the contact between the permeable canga and the less permeable altered ore, which act as a focal horizon for iron evacuation through discharge of a temporary perched aguifer (Bertachini et al., 2018). The vast majority of caves in all three areas open at the scarp's face (Fig. 4). Collapse of cave ceiling at the scarp can result in the arcuate retreat of the scarp, a feature especially common in Carajás, termed as amphitheater (Fig. 5C). Of note is the frequent occurrence of previously nondescribed crescent-shaped "cusps" (Fig. 5A) at the border of Carajás plateaus. They are largely responsible for the irregular pattern of some plateaus. These ubiquitous features, although an order of magnitude larger, bear resemblance to cave amphitheaters. The possibility that cusps are formed through coalescence of smaller amphitheaters would place cave processes as major triggers of IF landscape evolution, a topic that deserves further research. Soil washed from the caves generates a small vegetation-rich flat zone at the scarp front, representing a break in the steep profile of the slope.

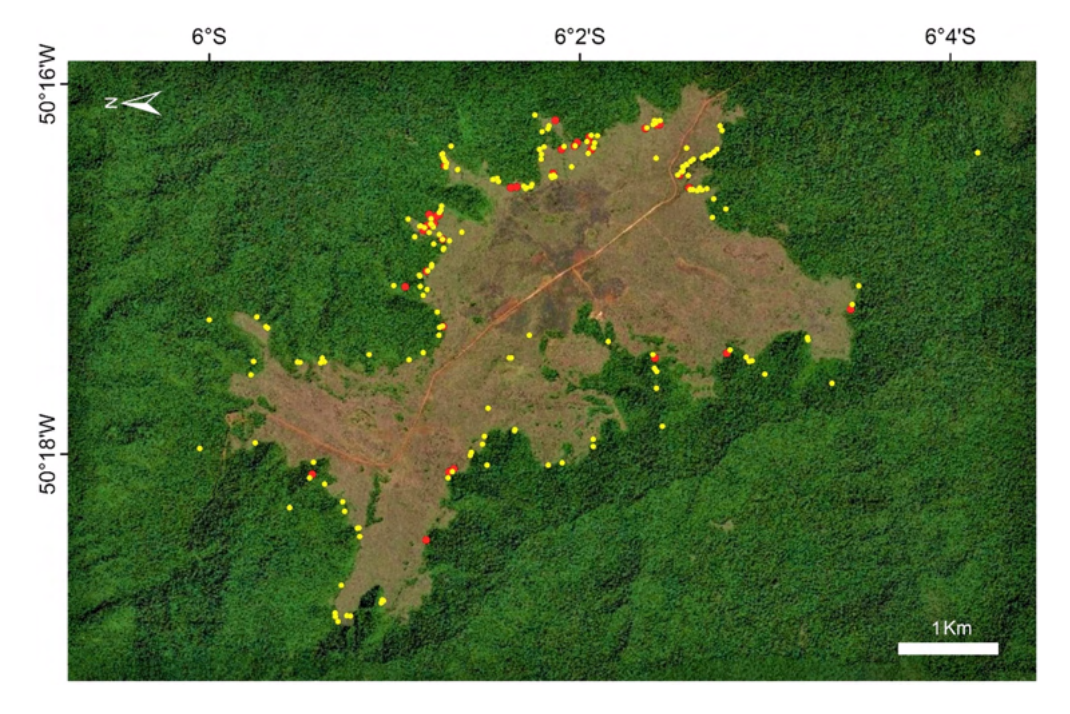


Fig. 4. Aerial view of N1 Plateau, North Ridge, Carajás with the canga outcrop (light grey) surrounded by Amazonian rainforest. The image shows that the location of cave entrances (yellow dots) are nearly always associated with scarps at the limit of the canga cap. Larger (>50 m long) caves are marked with a red dot. Image from Google Earth and cave locations from the Brazilian cave database (CANIE).

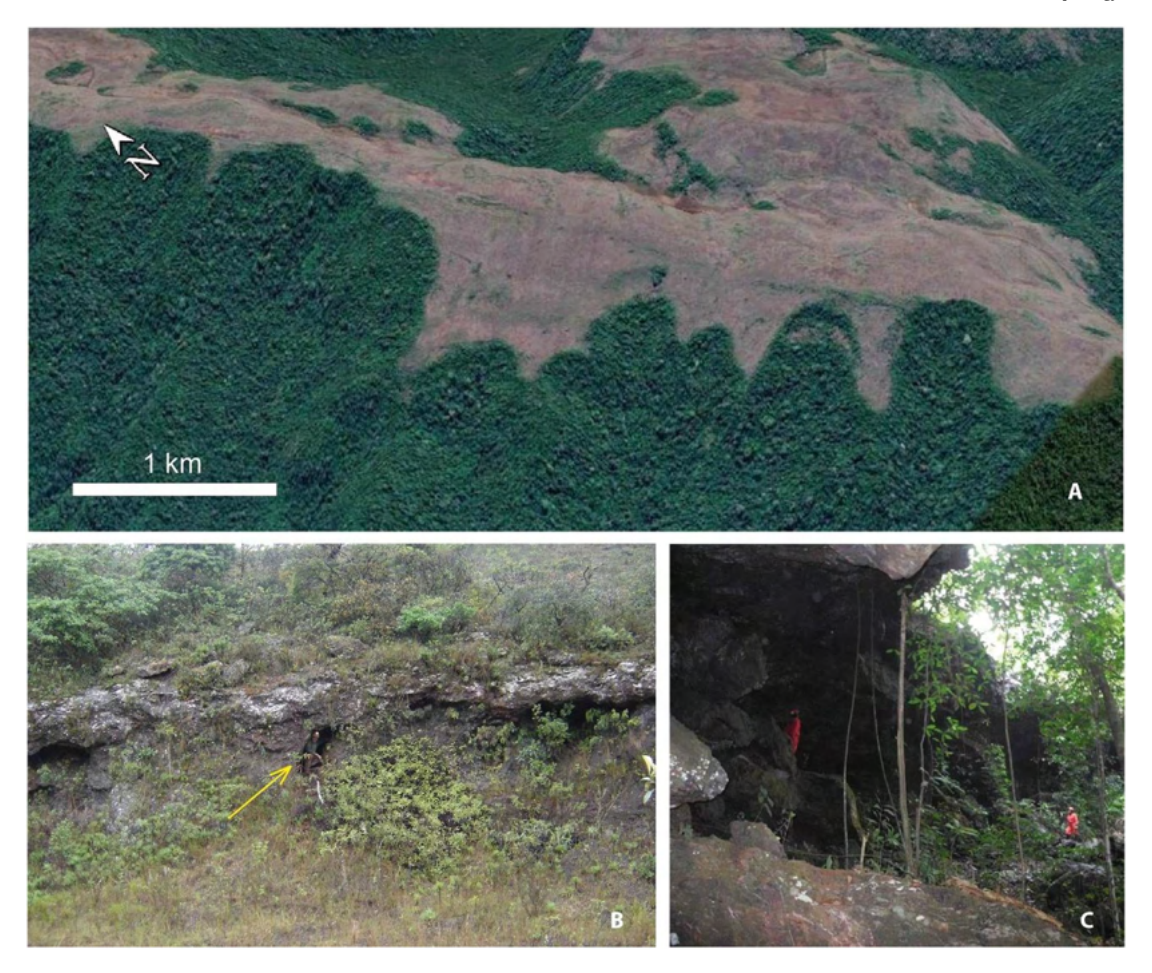


Fig. 5. (A) Sequential "cusps" commonly mark the boundary of canga plateaus as shown in this oblique SE trending view of the South Ridge in Carajás. They may represent macroscale analogues of cave amphitheaters. Google Earth image with 3× vertical exaggeration. (B) A typical scarp in the IQ. Arrow points to a person inside the cave. (C) Cave amphitheater associated with collapse of an entrance room in Carajás.

4.3. Geological controls on cave dimension

Table 2 updates a previous study (Auler et al., 2019) and allows for a dimensional analysis of caves in terms of geological context for the study areas. Caves can occur (i) entirely within canga, (ii) within weathered BIF, or (iii) at the contact between these two IF rock types. Our cave data set exhibits a large dominance of small caves (median length of 15.9 m), with the longest cave being only 372 m long. All three areas display the same distribution pattern, with a limited number of caves being over 100 m long (Fig. 6). Mean/median values for Carajás, IQ and SE are respectively 32.5 m/18.5 m, 21.0 m/12.4 m and 18.3 m/12.2 m.

The Carajás region has the larger caves in all three dimensional parameters (length, area and volume) (Table 2, Fig. 7). In Carajás, the area/length and volume/length ratios are significantly higher than in the IQ and SE, which display similar values. The high values for cave volume in Carajás caves are particularly conspicuous, with volume per unit length over twice as much (mean of 7.3) as in the other two areas (mean of 3.1 and 2.8 respectively for IQ and SE). The distribution of caves regarding lithological context (Table 2) shows that dimension positively correlates with the contact between canga and the weathered BIF (Fig. 8). This lithological contact presents the largest caves in all three areas, although in Carajás and IQ it does not hold the largest number of caves. Dimensional difference is especially significant in Carajás, with mean values being nearly 100% larger for caves located at the contact, when compared to caves entirely in weathered BIF or canga (Table 2). Caves in canga and in weathered BIF display similar mean values. This may be explained by the fact that the canga cap is of limited

Table 2Dimensional data for caves in Carajás, IQ and SE.

	Cara	jás					
	n	Length (m)	Depth (m)	Area (m²)	Volume (m³)	Area/length	Volume/length
Canga	552	26.13	3.53	102.9	183	3.94	7.00
Contact	255	52.08	6.49	205.1	404	3.94	7.76
Alt. BIF	348	3 28.35	3.80	102.8	204	3.63	7.20
Total	1155	32.53	4.27	125.4	239	3.85	7.35
	Iron Quadrangle						
	n	Length (m)	Depth (m)	Area (m²)	Volume (m³)	Area/length	Volume/length
Canga	170	20.19	2.51	51.0	57	2.53	2.82
Contact	79	27.47	3.02	66.2	82	2.41	2.99
Alt. BIF	155	18.65	4.08	48.4	68	2.60	3.65
Total	404	21.02	3.21	53.0	66	2.52	3.14
	Sout	hern Espir	nhaço				
	n	Length (m)	Depth (m)	Area (m²)	Volume (m³)	Area/length	Volume/length
Canga	57	14.38	2.21	34.1	34	2.37	2.36
Contact	109	22.04	3.89	57.8	53	2.62	2.40
Alt. BIF	105	16.44	3.31	44.5	58	2.71	3.53
Total	271	18.27	3.31	47.7	51	2.61	2.79

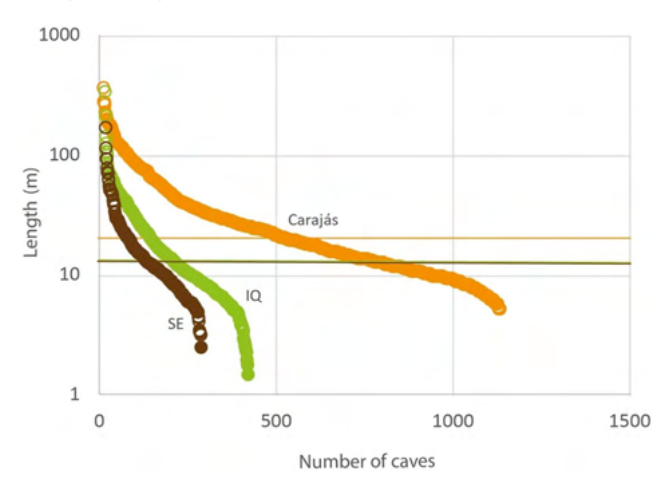


Fig. 6. Cumulative frequency graph (log scale) of cave length at Carajás, IQ and SE showing that small caves predominate in all areas. Light colored upper horizontal line represents mean values and lower green line the median.

thickness, somewhat restricting the dimensional expansion of caves, while the lower altered IF is less cohesive and may not be stable enough to sustain large continuous voids.

In Carajás and SE the difference in elevation between the highest and lowest point in the cave (depth) is more pronounced for caves at the contact. This is probably due to the fact that the canga layers tend to follow the slope and these caves normally display inclined passages (see Section 5.1 and Fig. 11).

An analysis of cave maps shows that the cave's plan configuration is spatially linked to the scarps. Caves normally develop at a right angle relative to the scarp line, but never extend beyond 100 m perpendicular (up-slope) from the scarp. This is a clear indication of a genetic relationship between caves and scarps as will be discussed later.

5. Morphology of if caves

Most caves in our data set are too small to reveal characteristic morphological features or even a more general plan pattern. We have thus selected caves which are longer than 50 m, totaling 238 caves for this analysis. Examining the plan map of these caves it becomes clear that they do not conform with the widely used patterns for carbonate caves which are largely controlled by groundwater recharge characteristics and dominant initial porosity (Palmer, 1991). IF caves are mostly extremely irregular, even when predominantly rectilinear. Most long caves are organized as a series of highly irregular rooms connected by narrow passages (Fig. 9). Piló and Auler (2005) have termed this pattern as "globular", but in reality these rooms do not adhere to a spherical globe-like or bulbous morphology. Instead, they are commonly asymmetric and display a series of small conduits and projections at floor and walls that result in a highly jagged perimeter. Cave plan morphology appears to comprise variants of only one situation, represented by the coalescence of larger rooms and narrow connecting passages. They

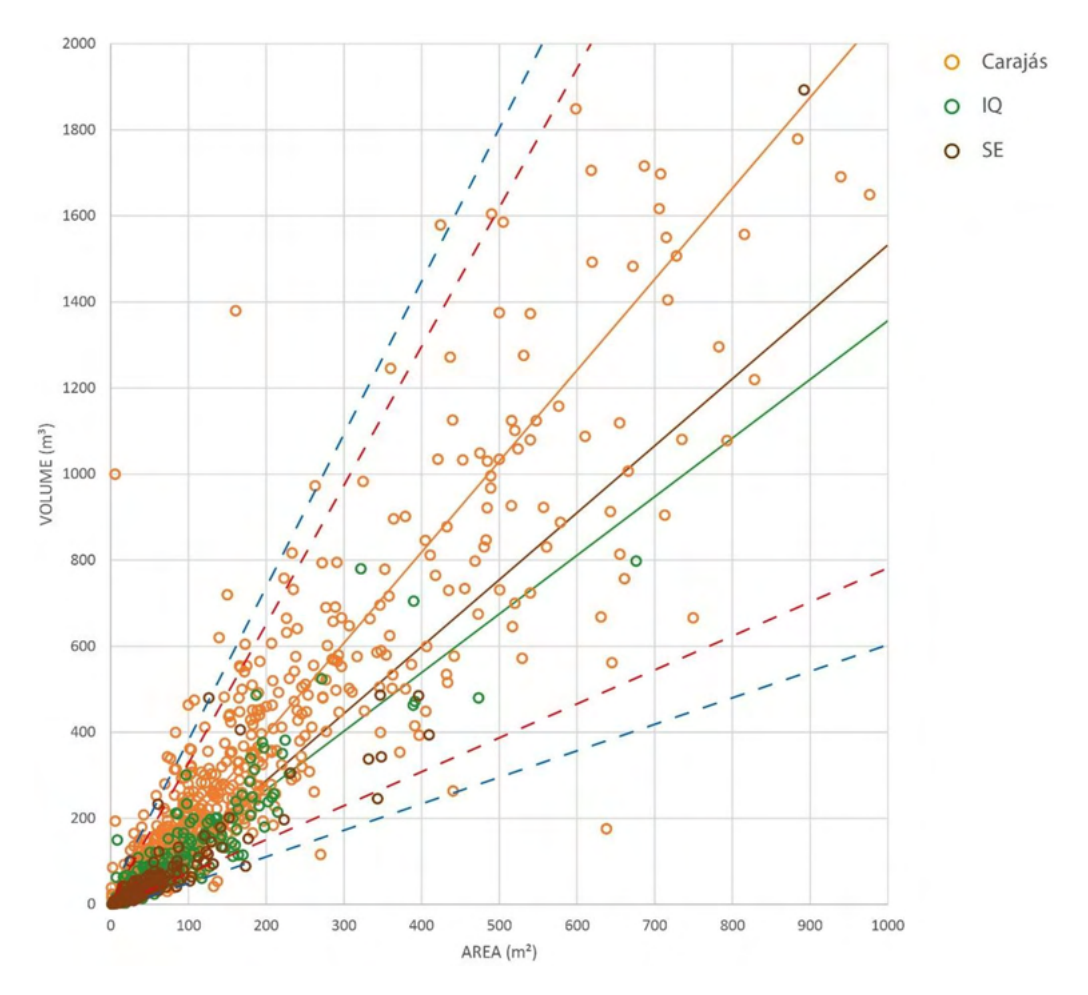


Fig. 7. Dimensional analysis of caves in Carajás, IQ and SE. Carajás has the largest caves (high volume/area ratio — see also Table 2). Linear regression for each region is shown in the corresponding color. Equations are y = 2.1135x - 26.606 for Carajás; y = 1.3629x - 6.294 for IQ and y = 1.556x - 23.18 for SE. Blue and red dashed lines represent respectively 99% and 95% percentilic confidence intervals.

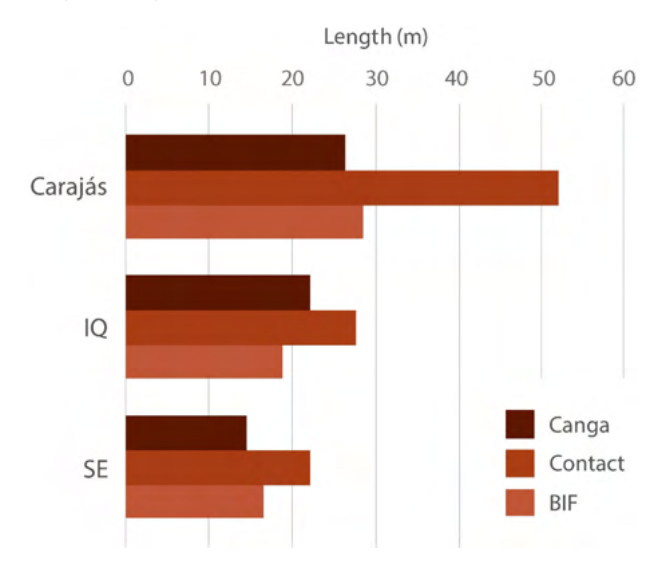


Fig. 8. Mean length of caves according to geological situations, showing that the contact between canga and weathered BIF favors longer cave development.

may develop both along one axis (normally following the slope gradient) displaying a rough rectilinear pattern that comprises the longitudinal connection of a series of connected longitudinal once independent rooms (Fig. 9B) or through lateral connections (Fig. 9A). Caves in canga display a more irregular pattern (Fig. 9C) both in plan and profile. In caves with multiple rooms, the narrow connection, if along the slope, is usually characterized by a steeper passage, while the rooms tend to be flat floored. The alternation between rooms and narrow passages also occurs at entrance level. Many caves show restricted entrances at the base of scarps (Fig. 9D), while others can only be accessed through

vertical collapse shafts, being originally devoid of a natural entrance. In Carajás approximately 50% of caves display an amphitheater at the entrance, showing that scarp retreat intercepted a room (Table 3 and Fig. 5C). On the other hand, narrow entrances are much more common in the IQ and SE areas (Table 3).

We have determined the number of rooms and narrow passages for each cave for our data set of 238 caves longer than 50 m, according to the example provided in Fig. 10. Data for the three areas (Table 4) shows that Carajás caves have, by far, the largest mean room area, although they present, overall, fewer rooms. Again, IQ and SE show approximately similar values, being slightly larger in SE. Caves located at the contact between canga and weathered iron formation always show smaller rooms, regardless of the region (Table 4). Caves in weathered BIF or canga show similar values.

Longitudinal profiles of IF caves display strong geological control (Fig. 11). Caves in the contact are dominantly characterized by ascending passages (Fig. 12) that follow the interface of canga (at ceiling) and weathered BIF (floor). These caves may display sections entirely in canga or in weathered BIF, and still retain their steep profile. Caves located entirely in weathered BIF tend to show a more level profile. Caves entirely in canga will conform to the local angle of the canga layer.

5.1. Fractal Dimension

Fractal is a multiscale geometry element used to describe forms in nature that are too complex and irregular to be described using simple Euclidean forms. Fractals were first described by Mandelbrot (1977) and further discussed in Mandelbrot (1983). Since then, many authors have used Fractal Dimension (FD) to analyze natural morphological features such as hillslopes, river patterns and cave morphology (Curl, 1986; Laverty, 1987; La Barbera and Rosso, 1989; Chase, 1992; Sagar and Chockalingam, 2004; Kambesis et al., 2016; Pardo-Igúzquiza et al., 2018).

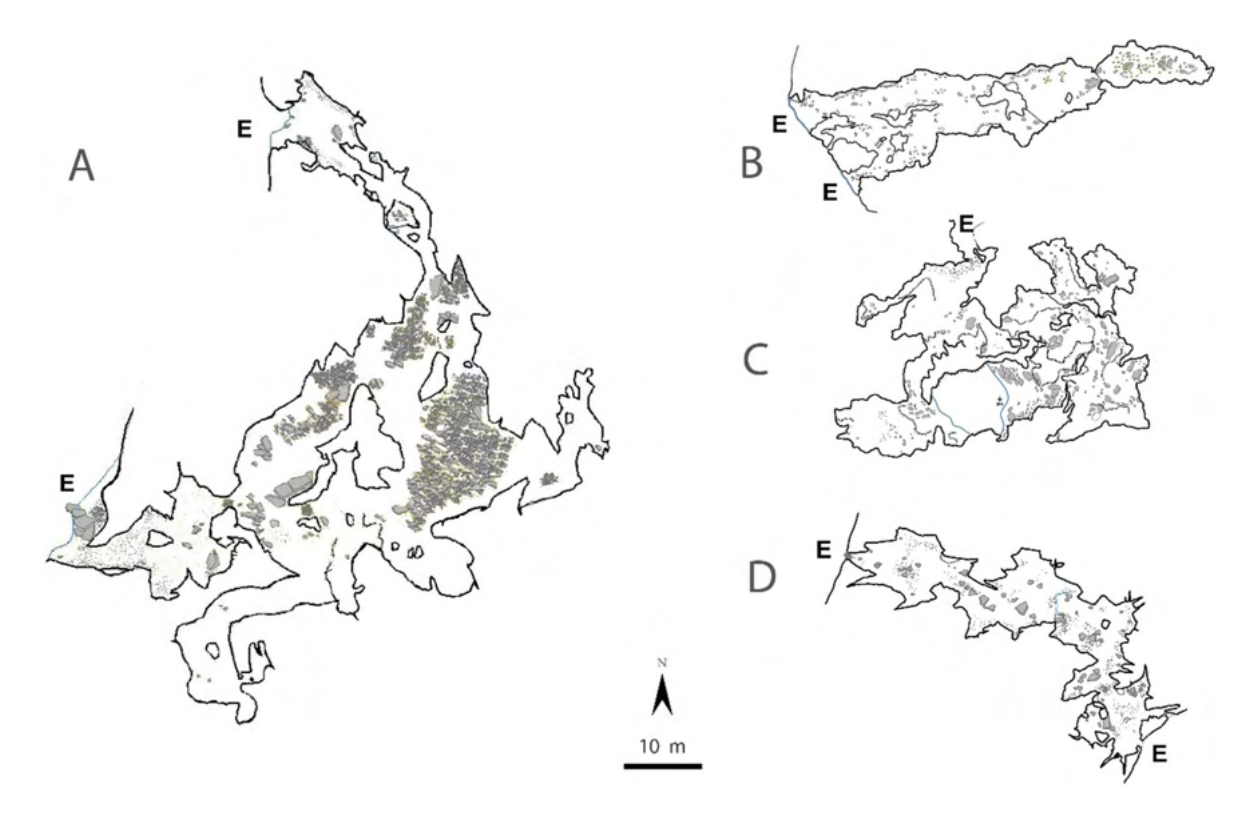


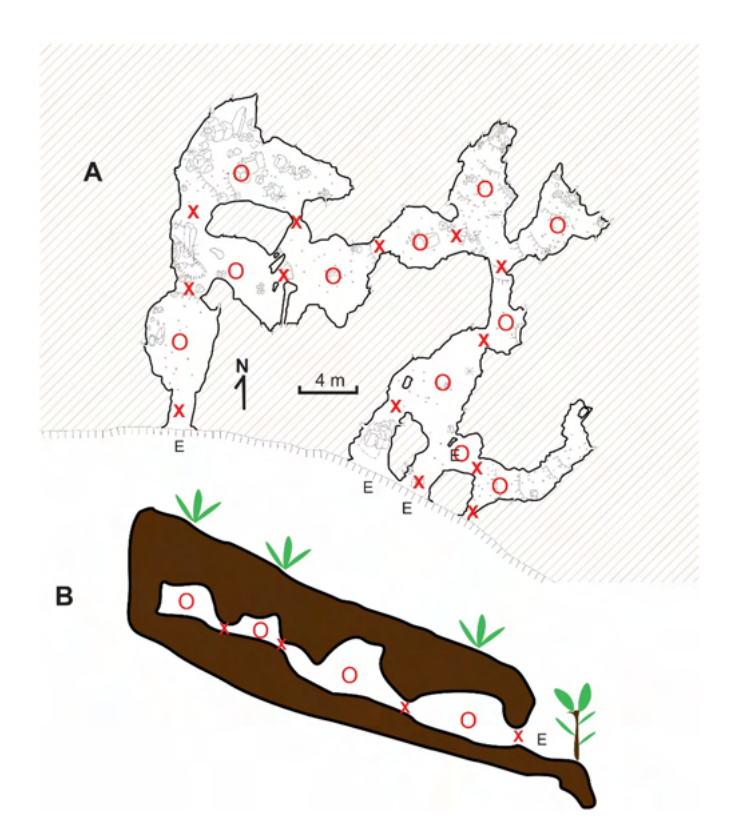
Fig. 9. Examples of cave plan patterns. (A) Cave in the North Ridge (Carajás) developed at the contact between canga and iron formation showing connection of multiple rooms by smaller passages both laterally and perpendicular to the scarp. This is the longest cave known in IFs with its 372 m in length. (B) A rectilinear cave in Bocaina plateau, Carajás, shows coalescence of rooms along one main axis. (C) A highly irregular cave in canga also at Bocaina ridge in Carajás. (D) An example of a cave in the IQ with very narrow distal opposite entrances. E — entrance.

Table 3Relative occurrence of entrance types (narrow entrances or amphitheaters/bisected rooms) in each geological context and IF region. Situations where the entrance is neither a clear amphitheater nor narrow are described as "Other".

	Amphitheater		Narro	Narrow		Other	
	#	%	#	%	#	%	
Carajás	95	51%	68	37%	22	12%	185
IQ	10	28%	19	53%	7	19%	36
SE	5	29%	9	53%	3	18%	17
Total	110	46%	96	40%	32	13%	238

The results obtained for 2D Fractal Dimension (FD) of caves are shown in Table 5, segregated by lithology, region and software. For FracLac, FD ranges from 1.3475 to 1.7653. The mean FD value obtained is 1.66 (rounded), regardless of the lithology. However, the FD range is lower for canga caves (0.2726) and larger for caves in BIF (0.4121). When comparing the three different regions, Carajás has the highest FD (mean of 1.6724) and the lowest amplitude of measurements (0.2726), while SE shows the lowest FD (mean of 1.5943) and the largest range (0.3546). IQ values lie in between (1.6469 – mean, 0.3045 range). FD results obtained by Fractal 3.4.7 are slightly different, ranging from 1.4278 to 1.7981. As for Fractal 3.4.7, the mean FD value obtained is 1.67 (rounded) regardless of lithology. Similarly, the largest FD range relates to caves in BIF (0.3471), although the lowest variation is observed at caves developed in the contact of Canga and BIF (0.2128). Concerning the studied regions, Carajás showed the highest FD (mean of 1.6781), while the IQ and SE show similar values with FD (mean) of 1.6499. The FD ranges are the lowest for the IQ (0.2471) and the largest for SE (0.3115).

Caves that develop in only one direction (linear caves) have lower FD than caves that develop in two or more directions. The irregular



 $\label{eq:Fig.10.} \textbf{Fig. 10.} \ (A) \ Plan \ view \ showing \ an example of the \ distinction \ between \ rooms, \ marked \ with \ "O", \ and \ narrow \ connecting \ passages \ (X) \ for \ a \ cave \ in \ the \ IQ. \ (B) \ Schematic \ profile \ view. \ E-entrance.$

Table 4Relative proportion of rooms in each geological context for the three IF study areas. Room area represents the maximum area, because the calculations include the entire area of the cave, since there is considerable imprecision in removing smaller passages (which however represent a minor portion of the total area) from cave maps.

Region	Geological context	Mean cave area (m ²)	Mean number of rooms	Mean room area (m ²)	Mean room area per region (m²)	Mean number of rooms per region
Carajás	Canga	469.8	4.8	111.6	97.9	5.5
	Contact	475.3	6.1	86.7		
	BIF	398.3	5.1	101.8		
IQ	Canga	228.5	7.8	34.8	33.8	7.4
	Contact	169.9	8.9	23.5		
	BIF	211.4	6	44.2		
SE	Canga	331.9	8	41.5	44.5	6.6
	Contact	236.2	7.1	34.2		
	BIF	303.6	5.2	67.9		

character (rugosity) of the walls does not show clear interaction with FD, nor does with the presence/absence of pillars. Caves with a prevalence of large rooms tend to have a higher FD than the ones with dominance of narrow passages. Pearson correlation was performed and the results are displayed in Table 6. According to the results, it is not possible to relate directly the size of the cave to the FD.

5.1.1. Lithological, geographical and morphological controls on FD

The 2D Fractal Dimension (FD) represents how a shape (in this case a cave layout) adheres to a predefined space (2 \times 1 proportion, 512 \times 256 pts). On one hand, the closer to 1 FD, the more likely that the shape will resemble a straight line. On the other hand, the closer to 2 FD, the space is more effectively filled by the cave layout (voids).

The results show that the lithology where the cave develops does not define its FD. On the contrary, the FD distribution is similar among the three rock types (Fig. 13). This is probably because iron caves are highly irregular, thus the lithology does not play a major role in defining the cave's fractal morphology.

On the other hand, the location, whether in Carajás, IQ or SE does play a role in its size and shape, hence in its FD (Fig. 14). Even though it has the largest sample, the FD variation for Carajás was the smallest among the three regions.

The role of cave morphology in the FD is shown in Fig. 15. The lowest and the highest FD values are shown at the left column. The right column shows three different caves, from the same region (Carajás), same lithology (contact) and with similar FD. It is possible to infer by

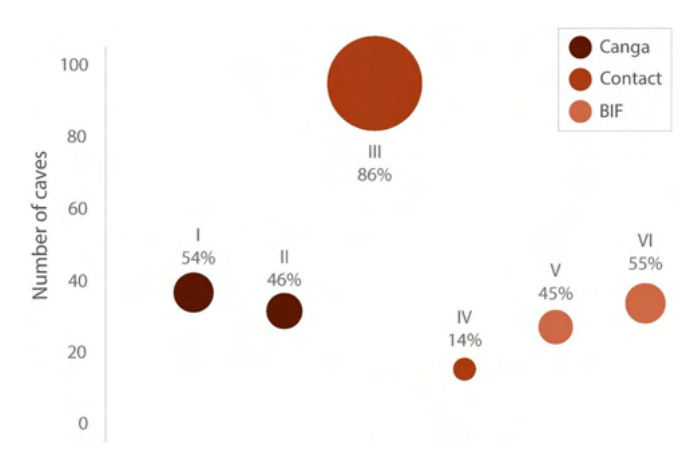


Fig. 11. Distribution of cave profiles in relation to geological context for the three areas combined. There is a clear dominance of steep ascending profiles in caves developed in the contact zone. I, III and V — inclined profile. II, IV and VI — flat profile.

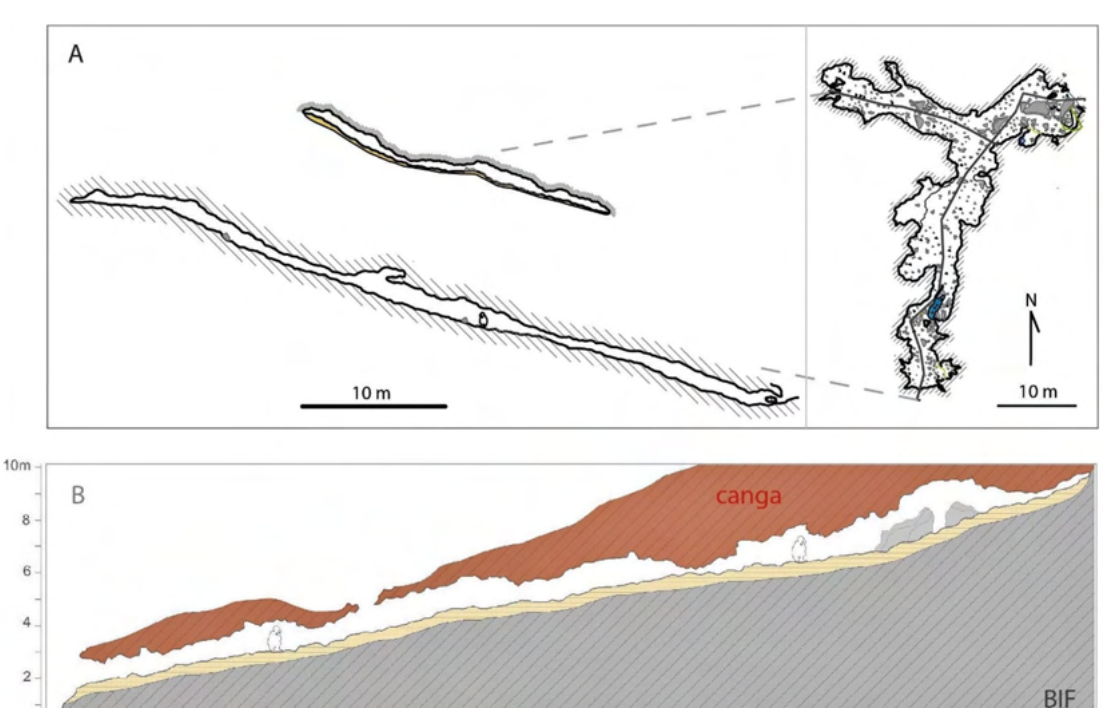


Fig. 12. Two representative ascending profiles. (A) Contact cave in SE, showing ascending profiles in both divergent passages. (B) Cave in the contact zone in IQ, showing ceiling collapse in the initial lower section.

analyzing this figure that caves with very different plan patterns can display similar FD. It is thus not possible to use FD alone to describe pattern or specific genetic processes taking place in IF caves.

Cave dimension does not affect the FD as shown by the Pearson correlation values (Table 6). This could be associated with the fact that fractal is a multiscale geometric element, meaning that the same shape would result in the same FD, regardless of its size. More important than the cave area itself, is how this area is distributed in a given space.

5.2. Underground landforms and sedimentation

0

Much of the highly irregular pattern of IF caves, represented by elongations in the cave perimeter, is due to the existence of numerous small conduits (canaliculi), normally at floor level, but also occurring along the walls and ceiling (Piló and Auler, 2005; Calux et al., 2019). These channels (Fig. 16A) may represent an earlier evolutionary stage of the narrow junctions, not wide enough to allow human access. IF caves show no evidence of dissolutional features (speleogens) which are common in caves formed by flowing water in most rock types. Rock projections oriented according to

the rock banding (in caves in weathered BIF) are common. The bedrock floor of IF caves is usually covered by sediment, but where exposed, can be very irregular, with jagged pinnacles (Fig. 16B) and basins (Fig. 16C). At the ceiling, the presence of pendants and pillars is characteristic, notably in canga (Fig. 17) which results in extremely irregular roofs. Pillars and pendants can be up to 3 m high, being limited by the cave height. Pillars do not display the common hourglass morphology as in sandstone caves (Aubrecht et al., 2011; Sauro, 2014; Bruthans et al., 2014) and can actually be inclined (Fig. 17D). The shallow nature of IF caves allows for the occurrence of ceiling collapse, which sometimes results in the opening of vertical entrances (skylights) (Fig. 12B). Roots commonly penetrate through the ceiling or entrance. Cave collapse is the major source of cave sedimentation, which is mostly autogenic. As mentioned earlier, the ascending (or flat) profile of IF caves does not favor the input of surface sediments, except near the entrance. Another major source of sedimentation is represented by the small channels. Some display a sediment fan at their mouth. The ironrich sediment coming out of these small conduits is highly sorted at fine-grained size, but may be soft and goo-like, especially in

Table 5Fractal Dimension for each lithology and region, calculated by FracLac and Fractal 3.4.7.

		Fractal Dim	Fractal Dimension (FD)								
		FracLac			Fractal 3.4.7						
		Min	Mean	Max	Range	Min	Mean	Max	Range		
Lithology	Canga	1.4927	1.6677	1.7653	0.2726	1.5090	1.6731	1.7981	0.2891		
	Contact	1.4551	1.6601	1.7537	0.2986	1.5498	1.6717	1.7646	0.2148		
	Iron Formation	1.3475	1.6626	1.7596	0.4121	1.4278	1.6709	1.7749	0.3471		
Region	Carajás	1.4927	1.6724	17,653	0.2726	1.5090	1.6781	1.7981	0.2891		
	Iron Quadrangle	1.4551	1.6469	1.7596	0.3045	1.5066	1.6499	1.7537	0.2471		
	Southern Espinhaço	1.3475	1.5943	1.7021	0.3546	1.4278	1.6499	1.7393	0.3115		

Table 6Pearson correlation for cave dimensional variables (length and area) and Fractal Dimension. Statistically significant values are shown with an asterisk.

Correlations	Length (m)	Area (m²)	Area/Length (m)	FracLac	FRACTAL 3.4.7
Length (m) Area (m²)	1 0.79*	1			
Area/length (m)	0.06	0.61*	1		
FracLac	0.06	0.17	0.20	1	
FRACTAL 3.4.7	-0.01	0.14	0.27	0.80^{*}	1

orifices in the walls or ceiling. Due to the absence of soil at the canga surface, this sediment can only originate from processes within the rock, as will be discussed in Section 6.2.

A peculiar feature of many IF caves is the occurrence of a crust coating the bedrock along the floor and walls. The crust smooths the cave contours and gives the walls a polished, lustrous appearance (Fig. 18). Mineralogical studies have revealed that the crust coating is mostly comprised by Fe(III) oxides and phosphates (Albuquerque et al., 2018). The coating can be found throughout the caves although it usually predominates at the distal portions, where environmental conditions tend to be stable, with relative humidity close to 100%. These distal passages are sometimes the hibernaculum of bat colonies, which has led to the association of phosphate crusts to reaction of bedrock with bat guano (Simmons, 1964; Albuquerque et al., 2018; Figueira et al., 2019). However, as will be demonstrated in Section 6.2, the iron oxyhydroxide crust has a complex origin and its development is linked to the growth and stabilization of the cave itself.

6. Generation of porosity and speleogenesis

There are a number of physical, chemical and biological processes that may account for porosity generation in IFs. These processes may take place over long timescales and depths, affect diachronically different portions of the rock unit and may act under both oxic and anoxic conditions. Rosière et al. (2008) point out that gradation from the original BIF to the high grade ore involves long term hypogene processes starting in the Proterozoic followed by supergene enrichment processes that evolved to the present day. These processes include remobilization of iron and leaching of gangue minerals (e.g. quartz, carbonate, amphibole), resulting in an increase in rock porosity (Ribeiro et al., 2021). Several distinct geochemical and microbiological mechanisms can account

for the complex transformation of BIF into a more porous Fe-rich rock and their relative importance may vary according to the environment in which they take place. The competing or interdependent role of these processes may bear relation to the evolving geochemical gradients that necessarily occur during the long history of the evolution of the IF deposits. Nonetheless, it is clear that the observed micro porosity and caves are the result of a complex suite of interrelated and still little known mechanisms that evolved with various intensities over vast timescales. The most relevant to void generation will be discussed in detail.

6.1. Initial porosity

The initial porosity may occur at depth and is not associated with the surficial canga deposits. In the IF regions of Brazil, entranceless voids have been routinely intercepted by drilling (Maurity and Kotschoubey, 1995) sometimes at depths of up to 600 m below the present surface (Rios and Santos, 2015). This deep origin of IF caves has led to analogies with carbonate hypogene cave morphologies (Auler et al., 2014). IFs generally contain productive aquifers suggesting porosity, and much of the available hydrogeological data comes from large scale dewatering projects required for the operation of deep open cast mines. Median outflow of springs is 400 m³/day reaching as much as 12,000 m³/day (CPRM, 2004). A dual porosity aguifer, IFs have components of a granular (in porous IFs) and fractured aguifer (in compact or little weathered BIF) (Chiste-Costa, 2017; Goncalves et al., 2018), which results in heterogeneous hydrogeological behavior. In BIF and hardened IFs, a correlation between fracture frequency and hydraulic conductivity has been observed (Carneiro et al., 2016). This anisotropy is also expressed according to the direction of the banding or foliation, with values of hydraulic conductivity 3× higher along these structures (Mourão, 2007). Preferential groundwater flow is thus focused along enlarged horizons represented by the rock banding and fractures (Mourão, 2007; Bertachini et al., 2018).

The extreme values of hydraulic conductivity are due to porosity at depth, which imply the generation of voids (Amorim et al., 2001). Carbonate facies are known to occur in certain portions of BIF deposits in the IQ (Dorr, 1964; Spier et al., 2007) and Carajás (Guedes et al., 2013) and the removal of the soluble carbonate has been invoked as an important mechanism of porosity generation (Simmons, 1963; Rosière et al., 2008; Monteiro et al., 2018a). Ribeiro (2003) has calculated that the net dissolution of carbonates, and then silica, can result in the creation of low density zones with up to 40% overall decrease in rock unit volume;

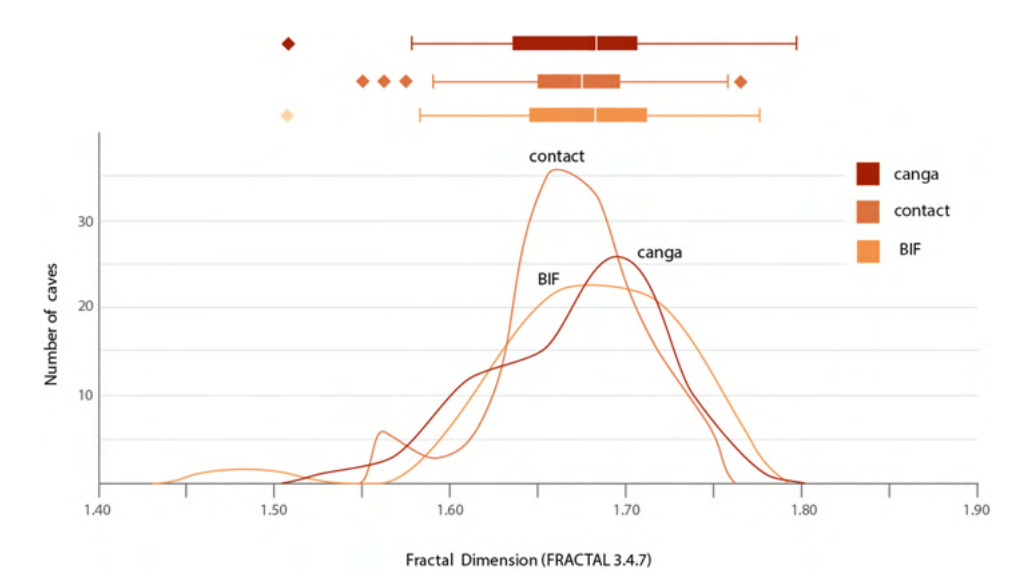


Fig. 13. Distribution of caves according to their geology and FD (Fractal 3.4.7).

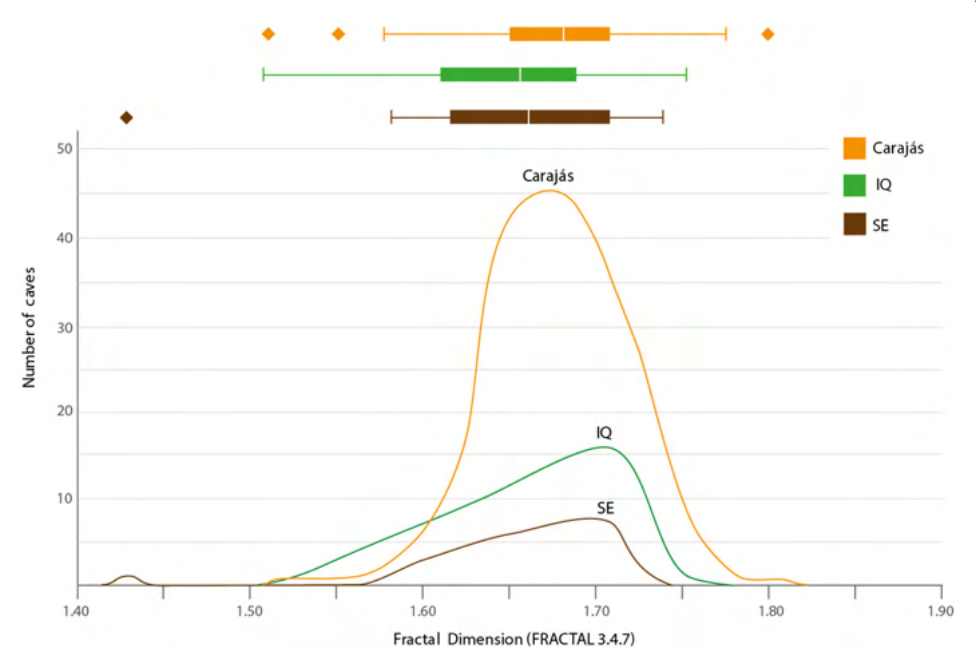


Fig. 14. Distribution of caves according to the region and FD (Fractal 3.4.7).

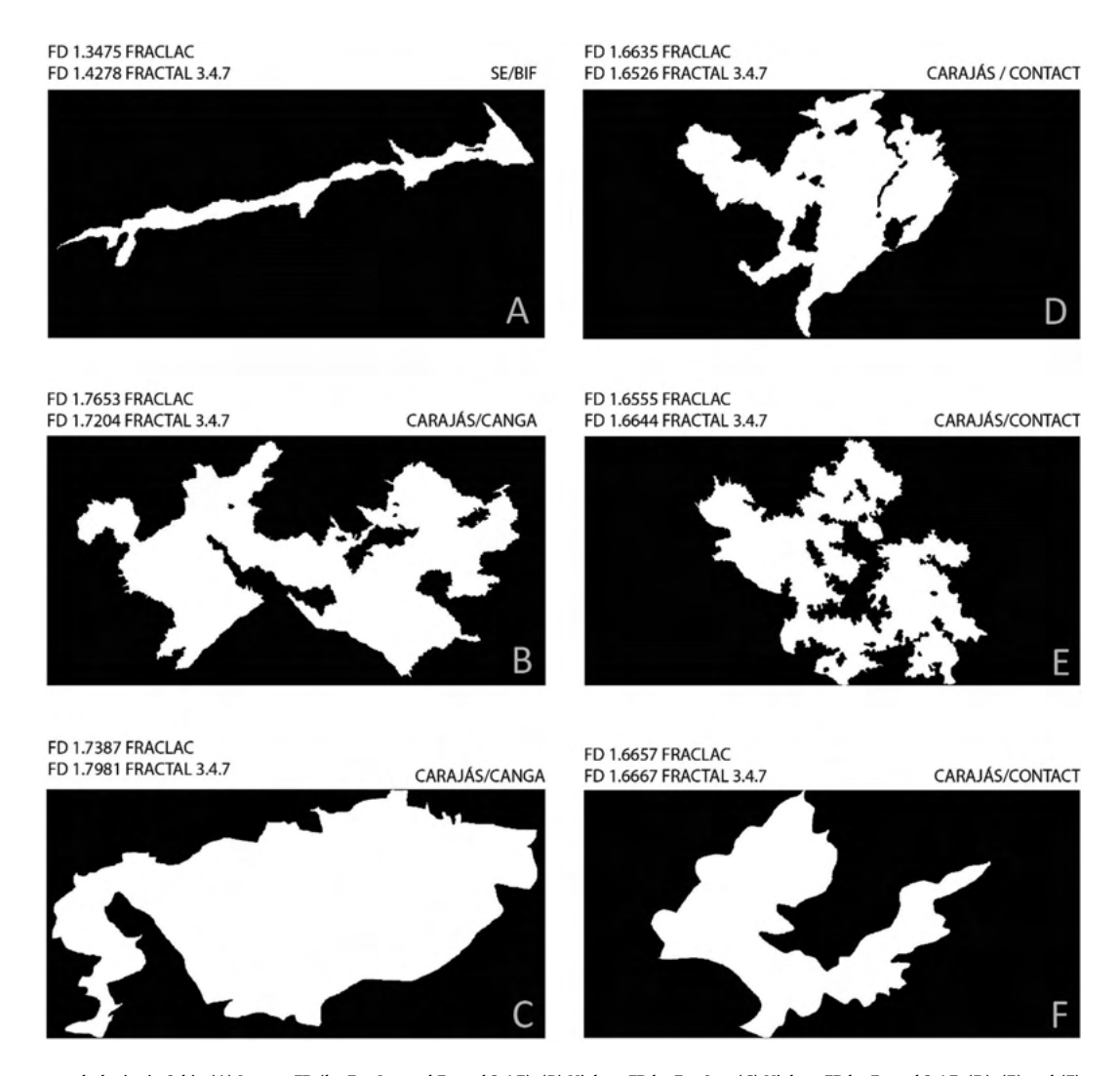


Fig. 15. Diverse cave morphologies in 8-bit. (A) Lowest FD (by FracLac and Fractal 3.4.7). (B) Highest FD by FracLac. (C) Highest FD by Fractal 3.4.7. (D), (E) and (F) represent caves with similar FD but very different shapes.



Fig. 16. Morphological features of IF caves. (A) Small channels at the floor level in a cave in the IQ. (B) Jagged floor, with pinnacles and projections in a cave in Carajás. (C) Sequence of rounded basins which fill intermittently in a cave in Carajás.

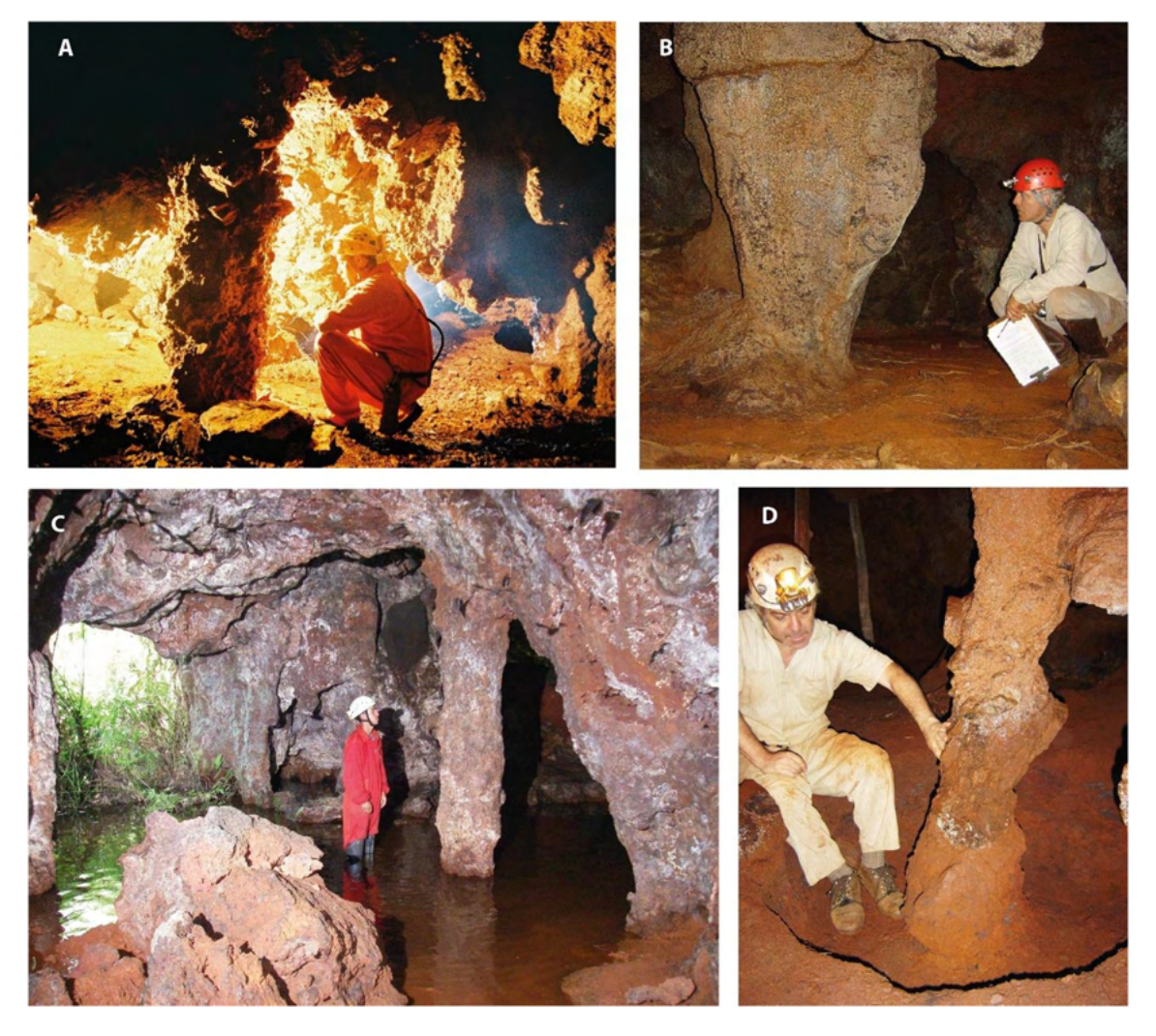


Fig. 17. (A) Pillars and pendants in a cave in IQ. Photo by Ataliba Coelho. (B) and (C) Pillars in caves in Carajás. (D) Excavated pillar in a cave in IQ.

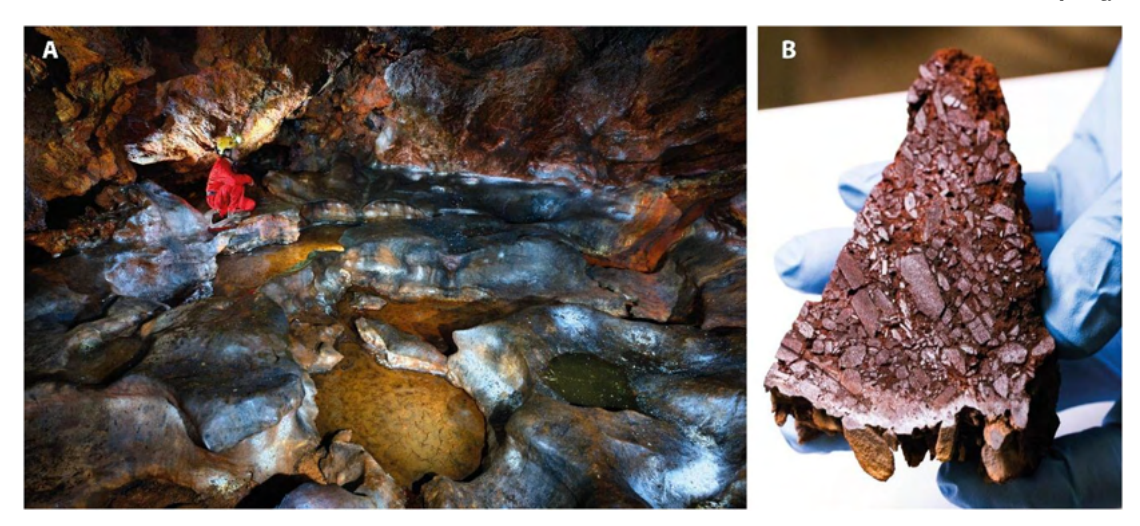


Fig. 18. (A) Coating by iron oxyhydroxides and phosphates produces a crust that smooths the irregular cave floor as in this cave in SE. Photo by Luciana Alt and Vitor Moura. (B) A polished section of cave wall in IQ, showing induration due to the development of crust (whitish layer) at the outer (lower) surface of the sample.

however, in the majority of the IF deposits, silica and iron are the major constituents and carbonates are largely absent. Silica dissolution is a well-known process (see review in Crundwell, 2017 and references herein) responsible for generation of large scale cave and karst features worldwide (Wray and Sauro, 2017; Auler and Sauro, 2019). Silica dissolution is particularly favored under high temperature and pH (Lunevich, 2019) along with organic leaching, which may explain the abundance of silica karst in warmer areas (Wray and Sauro, 2017). Being a slow process, regions under long term geomorphic evolution, especially in wet climates, commonly display developed silica dissolution landforms (Auler and Sauro, 2019). Silica dissolution does not necessarily imply surface (meteoric) sources of alkalinity due to its positive correlation with temperature. As such, dissolution could occur at depth aided by geothermally heated groundwater, which has been associated with the generation of caves and dissolutional features deep below the surface in quartzite and sandstone (Sauro et al., 2014; Suchý et al., 2017).

The preferential chemical leaching of silica, when in association with iron, is a key process in porosity generation in IFs. Numerous studies have stressed that silica solubility in groundwater can be substantially enhanced in the presence of iron, and iron solubility (and Fe(II) stability) can be enhanced when complexed with silica (Reardon, 1979; Morris and Fletcher, 1987; Baumgartner and Faivre, 2015; Kinsella et al., 2016 and references herein). Conversely, the presence of quartz can also mediate the removal of iron from solution (Sasowsky et al., 2000). Thus, silica removal and iron mobilization may take place abiotically under phreatic conditions in the early stages of porosity generation. The various silica phases behave differently in regard to geochemical mobilization. Abreu et al. (2016) have shown through petrographical studies in Carajás that silica dissolution follows a sequential path involving initially chert dissolution and then chalcedony/jasper, progressing from the center towards the border of the silica bands, creating voids that will eventually be enlarged through coalescence. The same study showed that less soluble minerals (including hematite) cause deviations in the dissolutional route. Abiotic transformative processes also take place within the Fe constituents. In particular, it has been noted in the IQ that the transformation of magnetite into hematite or martite in oxidizing environments may promote the dissolution of iron oxyhydroxide minerals, resulting in volume reduction within the IF rock mass (Lagoeiro, 1998; Rosière and Stacey, 2018). A review of chemical reactions in Brazilian IFs involving the various Fe and Si phases is presented in Monteiro et al. (2018a) and more comprehensive general reviews can be found in Cornell and Schwertmann (2003) and Baumgartner and Faivre (2015).

Void generation also takes place in the vadose near-surface environment. The transformation of the mostly insoluble ferric Fe(III) into the

soluble ferrous Fe(II) is a critical step in promoting the mobility (and later the reprecipitation) of iron in the shallow canga profiles, where most micropores and caves occur. Extensive microbially mediated transformations clearly occur in IF cave systems, including Fe(III) reduction (Parker et al., 2018; Gagen et al., 2019a, 2019b; Calapa et al., 2021) and Fe(II) oxidation (Levett et al., 2020a, 2020b, 2020c). The presence of oxygen prevents microbially mediated Fe(III)-reduction (Weber et al., 2006) preventing iron-reduction from occurring on surfaces within the caves. Instead, Fe-reduction is occurring behind the wall (the Feoxide crust) that is present on cave surfaces (Fig. 18). The iron-oxide crust prevents diffusion of oxygen, and the material in the caves behind this crust is soft (with a toothpaste-like consistency) and contains a high $(\sim 1 \times 10^7 \text{ cells/g})$ microbial cell count (Calapa et al., 2021). This material is termed sub muros (Latin for 'behind wall') and appears to be the primary site of Fe-reducing activities, dramatically reducing the amount of Fe(III)-oxides and increasing porosity (Fig. 19, Parker et al., 2018, Calapa et al., 2021). The importance of bacterially mediated redox reactions in the canga profile has been stressed by Parker et al. (2013a, 2013b, 2018), Levett et al. (2016), Monteiro et al. (2018a), Gagen et al. (2018, 2019a) and Paz et al. (2020).

The growth of microorganisms behind the wall appears to be fueled by organic carbon brought in from the landscape above by meteoric water, which percolates into the sub muros zone (Parker et al., 2018). Behind the oxide crust, and in the absence of oxygen, the microbial community uses Fe(III) as the primary electron acceptor for growth, with the generation of soluble Fe(II) (Parker et al., 2018). This process is supported by the observed microbial communities found in the sub muros, which are enriched in microorganisms encoding iron-binding oxidases (Parker, 2018). Nonetheless, the production of excess Fe(II) in solution could cause passivation of the Fe(III) oxides and limit reduction. To test this, Calapa et al. (2021) investigated the effect of punctuated waterflow, as would be encountered during the wet/dry seasons found in Brazil, on dissolution. These studies, which used columns of powdered canga, demonstrated that periodic flushing of the system dramatically enhances dissolution and increases porosity (Calapa et al., 2021).

The Fe(II) released by microbial Fe-reduction may remain in solution in the anaerobic *sub muros*, or alternatively, will react with the cave air, auto-oxidizing back into Fe(III). This turnover of Fe (Levett et al., 2016; Gagen et al., 2019b; Levett et al., 2020b, 2020c) may also be responsible for the observed microscale "turnover" of canga, while the generated oxides may enhance its durability (Monteiro et al., 2014; Monteiro et al., 2018a, 2018b; Levett et al., 2016; Gagen et al., 2019b; Levett et al., 2020b, 2020c). Additionally, microbial activities have been

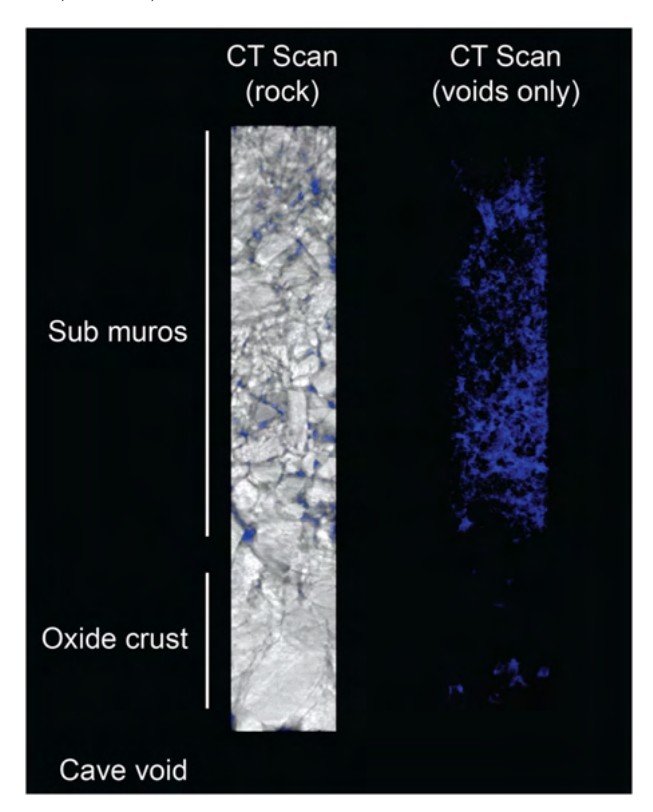


Fig. 19. Computed Tomography (CT) scan of the cave wall (oxide crust) with the *sub muros* layer behind it. The Fe(III)-oxides (rock in grey and voids in purple) are shown in the full CT scan; however, when the rock is subtracted, leaving only the voids highlighted (purple) the increased porosity of the *sub muros* zone is clearly visible.

proposed as a means to reclaim canga damaged by mining activities (Levett et al., 2020a, 2021).

The extensive microbial Fe(III) reduction has been proposed as a mechanism for the formation of caves in IF (Parker et al., 2013a, 2013b, 2018; Parker, 2018). In this scenario, microbial activity continues to enlarge the sub muros, eventually the weight of the sub muric material or weakening of the Fe(III)-oxide crust is sufficient for the crust to give way, allowing the sub muric material to fall into the cave, enlarging the void. The exposed Fe(II)-rich sub muros is then exposed, auto-oxidizing and re-forming the crust. The formation of this crust re-establishes the anoxic conditions within the sub muros, allowing Fe-reduction to resume and the process to repeat (Fig. 20). This process could lead to the bead-on-a-string morphology of the cave passages, which form through a series of voids that collapse in on themselves, creating connected voids (Fig. 20). This hypothesis is supported by the oxide crust fragments found on the floors throughout these caves. The process may demonstrate a more substantial redistribution of Fe than the microscale cycling of Fe in canga, and the presence of these caves indicates the possibility of more extensive weathering of IF than previously appreciated, including a contribution to the supra iron ore bodies themselves.

6.2. Cave evolution

Macro pores and caves hosted entirely by fresh or weathered BIF, without canga association can have an origin linked to the ancient and long lasting geochemical processes outlined previously, as evidenced by the existence of voids intercepted by deep drilling. Later long-term vertical uplift and denudation will eventually bring these caves closer to the surface, even considering the very low denudational rates of IF regions. At shallower depths, voids will be under the influence of a weathering front controlled by a combination of microbiological,

geochemical and erosional agents. Canga is highly permeable, in marked contrast with the low permeability of the weathered ore. Vertical infiltration of water in canga can occur both through fissures or the matrix (Dias and Bacellar, 2021) and leads to the formation of a perched aguifer during the wet season (Bertachini et al., 2018), with downgradient flow along the canga/weathered BIF interface. The downslope hydraulic gradient can be significant, due to the often steep angle of canga slopes (see cave profiles in Fig. 12). Subsurface flow (interflow) along the canga/weathered BIF contact represents a powerful mechanism for the generation and enlargement of pores and caves. The integration of existing porosity with slope and surface hydrological processes is a key component of the later vadose evolution of caves (Auler et al., 2014) because it will supply the canga/weathered BIF contact not only with abundant organic matter, fostering dissolution and bacterially mediated processes, but also with erosional power, enabling the evacuation of insoluble material.

The concentrated austral summer rainfall in the IF regions in Brazil leads to temporary hydrological saturation of the canga pores, which will drain through vertical infiltration towards existing caves (Dias and Bacellar, 2021). Parker et al. (2013a) has shown that pH of infiltration water in IF caves can be as low as 2, and the amount of organic dissolved carbon is much higher than in carbonate caves (Parker et al., 2018). Besides mechanical removal processes downslope, the seasonal perched canga aquifer favors geochemical and bacterially mediated processes.

The peculiar sequential combination of larger rooms and smaller connecting passages (bead-on-a-string morphology) is highly suggestive of coalescence of previously isolated (at least in terms of human access) rooms (Auler et al., 2014). When the connection occurs between rooms located along the scarp (i.e. not uphill following the slope), the caves may grow laterally. The larger caves always display both lateral - and along the slope - connections (see Fig. 9). The basic, initial element of IF caves is, thus, the room, with the smaller connections and elongations representing later additions. We have quantitatively analyzed the relationship between narrow junctions and rooms for our data set of 238 longer caves (Fig. 21). There is a positive trend between number of rooms and mean length, showing that the coalescence of rooms plays a role in cave development (Fig. 21B). There appears to be a limit to the number of rooms, with most caves having between 4 and 6. This may be controlled by the elimination of rooms due to mechanical scarp breakdown, generating amphitheaters.

Caves located at the contact always display, regardless of the region, smaller room area than in the other geological situations, even when the mean cave area is larger (as in Carajás — Table 4). We interpret this as due to the modification of rooms by the interflow along the contact. In the other situations there will be less mechanical power to mask the original room morphology.

As mentioned in Section 6.1, mobilization of iron through Fe(III) reducing bacteria (Parker et al., 2013b, 2018; Calapa et al., 2021) is a powerful mechanism that aids in the formation and expansion of pores and caves. Of particular interest is the precipitation of iron at the cave inner boundaries (ceiling, walls and floor), generating a coating layer (Fig. 18). Similar crusts in non-IF caves are formed by precipitation of solid phases from aqueous solutions originating from chemically saturated infiltration water within the cave. Since coatings in IF caves cover most surfaces, including overhanging sections, and flowing water is observed infrequently over them, a normal percolation origin can be discarded. The bacterially driven mode of cave genesis, wherein microbial Fe-reducing activity behind the walls causes collapse and wall retreat (Fig. 20) benefits from the episodic hydrological saturation of the canga profile during the rainy season, allowing for ample input of organic carbon and removal of passivation by Fe(II) (Calapa et al., 2021).

Caves are thus protected by the iron oxyhydroxide crust and will mainly evolve through rounds of collapse of portions of ceiling and walls (Fig. 20). This will lead to further oxidation and crust precipitation in the newly exposed section. This may explain why the crust tends to

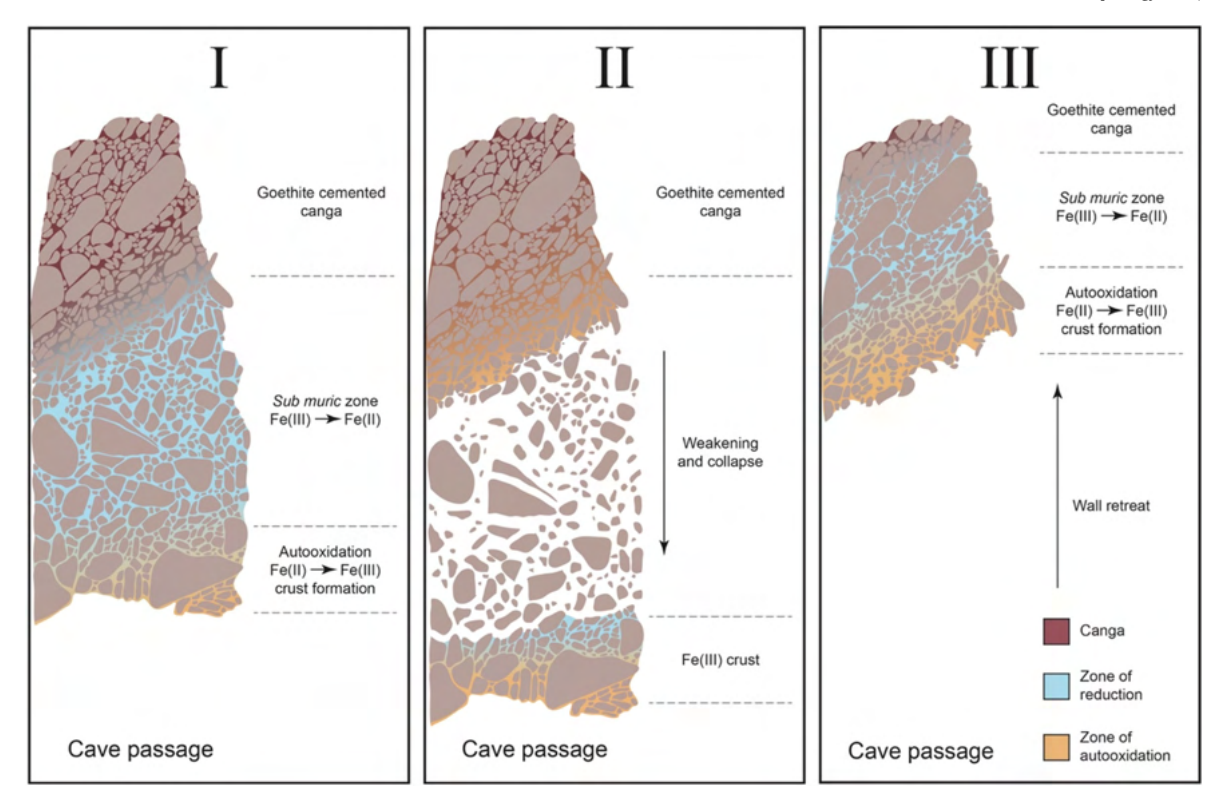


Fig. 20. The model for IF cave formation. Stage I. The autooxidation of Fe(II) exposed to oxygen in the cave passage creates Fe(III)-oxides that cement the passage walls into an ~2–3 cm thick crust, allowing anaerobic conditions to be established. Water percolating through the canga brings organic carbon-rich water to this anaerobic, sub muric zone, providing the reducing potential for FeRM to reduce the insoluble goethite cements to soluble Fe(II), which is removed by water flow. Stage II. Eventually, the loss of the goethite cements in the canga leads to a loss of structural integrity in the sub muric zone and the iron crust is no longer strong enough to hold back the wall, which collapses into the cave void. Stage III. Following collapse, exposure of Fe(II) fluids to oxygen reforms the Fe(III)-oxide crust, restoring anaerobic conditions behind the wall and the process repeats. Over time, repeated collapse leads to wall retreat and formation of the cave passages and observed morphology.

be thicker on the floor or on less inclined surfaces (see Fig. 18) because these areas are less prone to gravitational collapse. The *sub-muros* deposition of the crust is of paramount importance to cave preservation in the same way as surface canga promotes the long term resilience of iron surfaces. Without *sub-muros* coating, caves would likely have collapsed due to low mechanical stability of the mobile and sometimes soft iron constituents of the bedrock. This represents a novel mechanism of cave formation that enables IF caves and related porosity to survive over exceptionally long periods in the landscape.

As shown in Table 4, the elementary volumetric unit of IF caves – the room – has been shown to be significantly larger in Carajás than in the IQ and SE. The fact that there are still narrow connections between rooms, even in Carajás, demonstrates that they have not yet achieved their maximum possible volume, which would lead to coalescence and elimination of the connections. Larger rooms tend to be more unstable and thus a positive growth feedback can be created in Carajás, allowing for more frequent collapse and faster cave volumetric expansion. The ratio connections/rooms (approximately 1) is the same regardless of study area, showing that these parameters may not necessarily represent different stages of evolution. The existence of larger caves in Carajás can be explained by: (i) larger plateau areas which will provide a more extensive catchment area for interflow hydrological processes than in the less extensive ridges of the IQ and SE; (ii) much warmer climate, enhancing porosity development and cave formation; (iii) wetter climate which results in more water availability and increased runoff, favoring both chemical and mechanical removal of IF constituents and (iv) the availability of organic carbon under Carajás equatorial conditions which will catalyze redox and microbiological interactions.

The persistence of IF caves in the landscape also bears relation with the geomorphic evolution of the IF plateaus and ridges. Denudation in IFs terrains is slow due to the protective role of canga (Vasconcelos et al., 2019). However, scarp retreat is a dynamic process (Vasconcelos and Carmo, 2018) and, although canga can be regenerated within the weathering profile (Monteiro et al., 2018a), scarp rupture tends to be mostly a mechanical process, controlled in IF areas by vertical (aligned with the scarp) and surface-normal unloading joints frequent in nearly all caves and scarp zones. In this regard, caves in Carajás are in a more advanced dismantling stage, in which rooms are being exposed through scarp disintegration, generating amphitheaters (~50% of all Carajás caves), while in IQ and SE, the "original" configuration, in which connection with the surface occurs through narrow passages, still prevails (Table 3).

The genesis of pendants and pillars, always associated with canga ceilings (Fig. 17), cannot be linked to classical dissolutional mechanisms as in caves in other rock types. Gravitational percolation of water through the permeable canga may create vertically oriented redox zones within the rock, cementing clasts, and generating hardened "finger like" zones which are more resistant than the surrounding rock mass (Fig. 22). This process can be described as a vertically oriented sub-muros which will serve as an avenue to further catalyze oxidation and induration. In addition to gravitational infiltration, roots, tubules and plants can also serve as templates for iron oxide precipitation (Gagen et al., 2019b) and can help in the creation of these vertically oriented redox fronts. The conditions for generating pillars and pendants precede the formation of the caves, the pillars and pendants being "exhumed" due to the *sub-muros* sequential collapse. This mechanism bears resemblance to finger flow phenomena common in coarse soil profiles (Liu et al., 1994; Allaire et al., 2009; Wang et al., 2018).

Autogenic well sorted fine-grained sediment supplied by the small channels are ubiquitous in IF caves. As pointed out, due to the absence of soil above ground, they must result from microbiological reactions

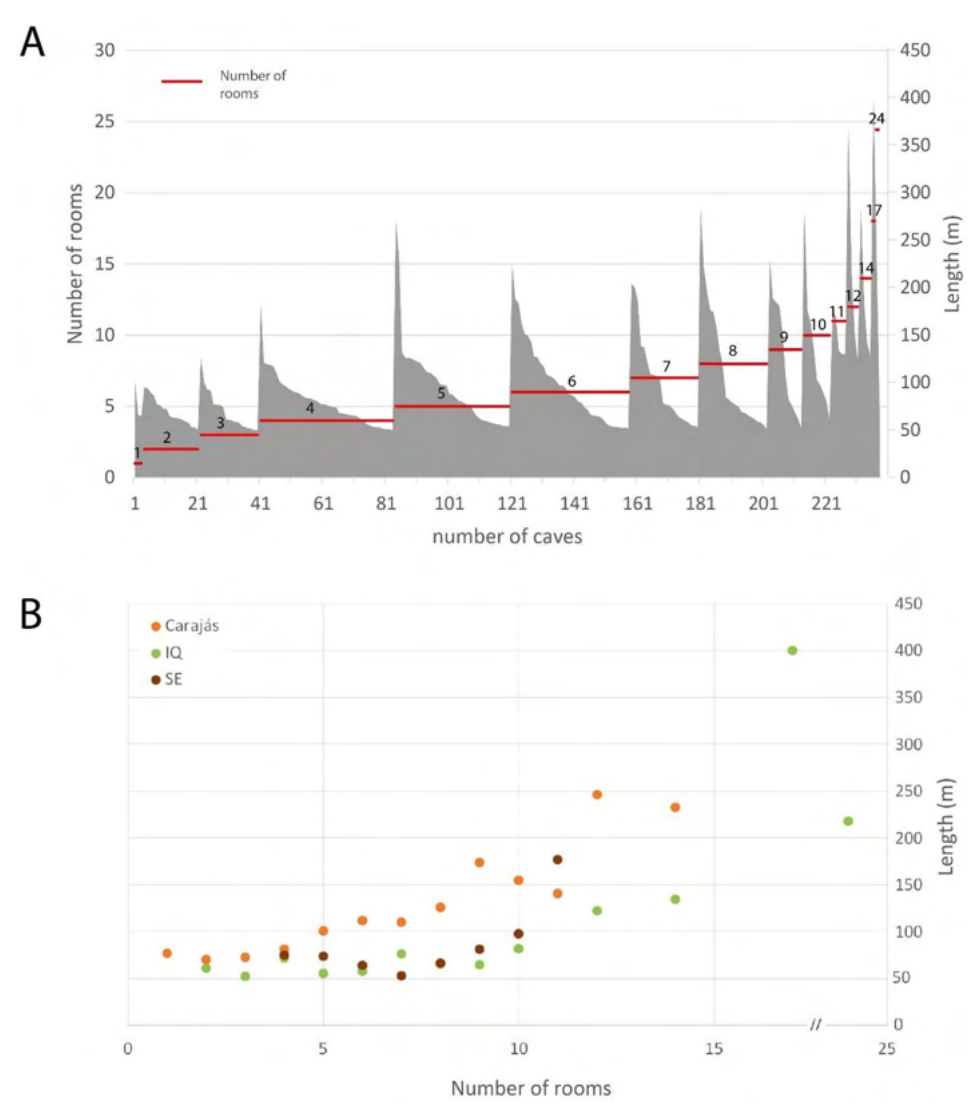


Fig. 21. (A) Combined distribution of caves per number of rooms for the three study areas. Length distribution in each room class (marked by a red line) follow a very asymmetric distribution similar to a Pareto (hyperbolic) distribution, typical for the statistical ordering of caves (Curl, 1986). Caves with 5 rooms predominate. (B) A similar analysis, but separated by area. Mean values show that cave length tends to increase with number of rooms in all areas.

within the rock mass and represent the non-soluble phase resulting from the process of porosity generation. Although Piló and Auler (2005) have suggested that piping processes could be responsible for sediment evacuation, this is not strictly the case, as Fe and Si mobilization and transport are related to a geo-biochemical front that advances towards the inner portion of the IFs plateaus and ridges.

In caves with limited or no soil it is possible to observe a highly jagged floor displaying pinnacles, deep cut basins and sharp projections (Fig. 16B, C), especially if there is active infiltration. This may be related to highly acidic dripping as demonstrated in one such cave (Parker et al., 2013a). Scherer (2017) hypothesized that, in Carajás, caves that display such jagged floor are located close to, and at lower elevations than, lakes and swamps, which could have favored the input of acidic and organicrich infiltration water. This relationship, however, is not observed in similar caves in the SE. Albuquerque et al. (2018) suggest that phosphoric acid derived from bat guano can also account for dissolution (and later precipitation) of iron oxyhydroxides. Bat guano has an important role in precipitating phosphate speleothems (Simmons, 1964; Albuquerque et al., 2018; Figueira et al., 2019) but their possible influence in cave expansion, if significant, will likely be obliterated by the associated constructional processes.

7. Iron mobilization and landscape evolution

IF landscapes evolve through a complex combination of geochemical and microbiological processes. The deep iron-rich profiles, generated by long term hypogene and supergene processes (Rosière et al., 2008), have been able to defy erosion not only due to their low geochemical rates of dissolution, but also due to the mobile and self-regenerating canga blanket (Dorr, 1969). The two major original constituents of the unweathered BIF bedrock, silica and iron, follow distinct geochemical paths throughout the long IF evolutionary history. Silica, relatively mobile in tropical temperatures, is the first to be removed by groundwater, resulting in the concentration of iron. Several authors (Ribeiro, 2003; Spier et al., 2003; Rosière et al., 2008; Rosière and Stacey, 2018; Ribeiro et al., 2021) have pointed out that silica (and if present, carbonate) leaching represents the first step, both for hypogene and supergene processes, towards porosity generation and, consequently, iron concentration. The early existence of a porous rock, even if not displaying voids large enough to be considered as caves, is an important condition for generating the highly transmissive aquifers typical of IFs (Amorim et al., 2001; Mourão, 2007) which allows for groundwater circulation and further Si leaching. The occurrence of deep weathered zones

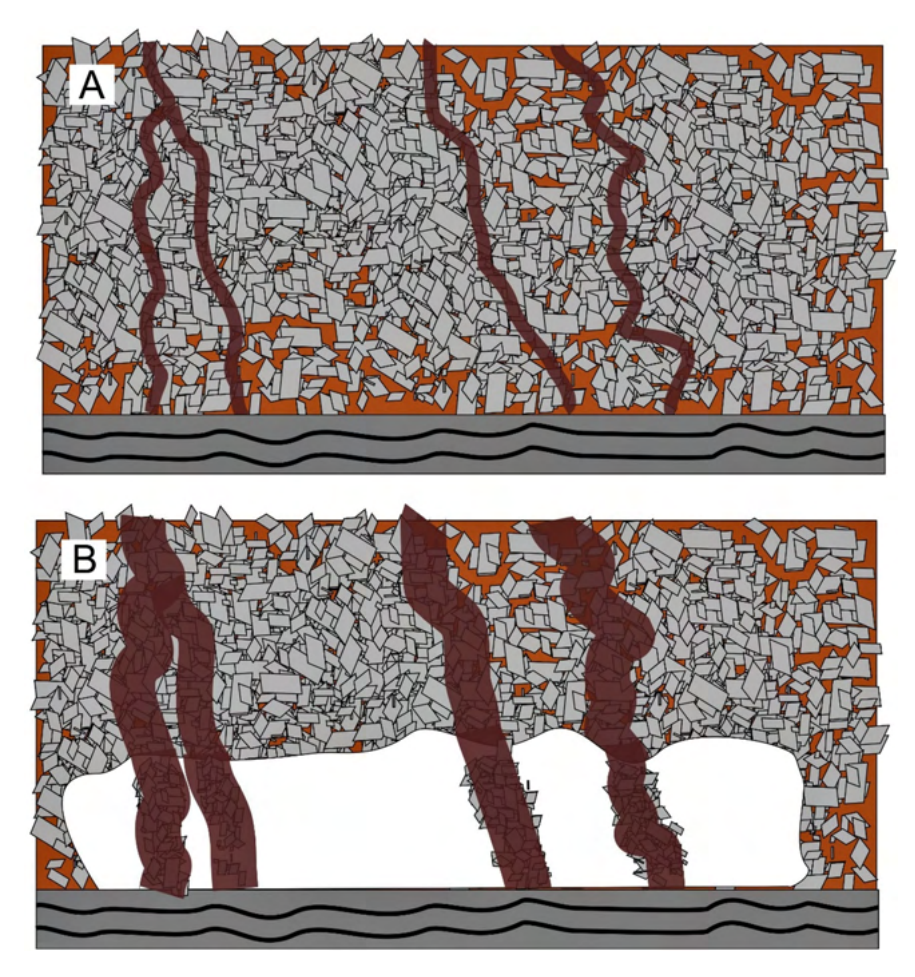


Fig. 22. Hypothesized finger flow genesis of pillars and pendants in IF caves. (A) Vertically oriented gravitational infiltration of water creates redox finger-like fronts. (B) Following generation of void (cave), exposure will lead to oxidation. These finger zones will be more resistant to collapse. Coating of sub-muros material will smooth the external surface of pillars.

along relatively fresh (unweathered) BIF (Rosière et al., 2008), shows the selective nature of the geochemical alteration front, which is controlled by groundwater flow and specific geological structures such as major faults and fractures, besides the more soluble avenues represented by the (silica) bands (Rosière and Stacey, 2018). In parallel with silica and carbonate leaching, the low Fe content characteristic of IF springs (Mourão, 2007; Carvalho, 2012; Chiste-Costa, 2017) indicates limited net loss of iron, suggesting that Fe tends to be remobilized within the system leading to iron concentration and the gradual generation of canga profiles and high-grade iron bodies.

Canga is a key component of the IF landscape. Although normally interpreted as being generated through surface-related processes (Simmons, 1960; Dorr, 1964; Spier et al., 2019), observations inside caves have demonstrated that the weathering front related to canga formation occurs also at depth and involves chemical, microbiological and mechanical processes as suggested by Monteiro et al. (2018a). The gradual change between a rock with leached silica, but with still recognizable relict banding structure, towards canga described by Dorr (1964), can be observed at various transitional stages (Fig. 23), generating what has been named by Dorr (1964) as "structured canga". This involves initially the fragmentation of the iron bands. Then, through collapse and translocation, the fragments lose their orientation leading to the chaotic arrangement of clasts typical of canga. Canga matrix can also vary from hardened to soft paste-like oxyhydroxide, depending on its redox state. In a few situations (as through collapse openings at ceiling or when the cave has an up gradient entrance) there may occur local transportation of sediment towards the caves. This sediment is easily distinguished from both canga and the fine-grained sediment derived from small channels due to its imbricated nature, and variation in particle size (Fig. 23A). The *in situ* induration of the previously unconsolidated iron-rich sediment results in what we name as "secondary canga" because it was formed later than both surface canga and caves, and can be positioned stratigraphically below the weathered BIF.

Rates of canga generation at the contact zone between canga/weathered BIF must be somehow in equilibrium with the very slow rates of surface denudation (Monteiro et al., 2018a), otherwise canga would have been gradually eliminated from the landscape, exposing the friable IF to erosion. The dynamic equilibrium between denudation and soil generation has been demonstrated for thick weathering profiles (Dosseto et al., 2008, 2011). The canga/weathered BIF contact zone will thus migrate downwards in time, in parallel with the slow dismantling of canga at the surface. The fact that the unconsolidated weathered BIF has survived for hundreds of millions of years attests to the long term existence of canga. The coating layer associated with the submuros can be interpreted as an underground, void (and rock) protective cover, which promotes the stabilization of the canga profile, protracting mechanical breakdown. Caves can, thus, evolve for long periods since their inception in the deep phreatic zone, much likely beyond the oldest ~70 Ma ages obtained from the self-healing canga profiles in the IF areas of Brazil (Vasconcelos and Carmo, 2018). These ever evolving Fe oxyhydroxide fluid migration zones will help indurate surficial and underground canga, as well as cave/pore outer surfaces, besides fostering the selective hardening of heterogeneous sections of the canga profile. Both canga and sub-muros layers represent sinks for the mobile iron and are genetically associated with high-grade supergene iron deposits.

Scarp disintegration appears to be a major controlling process in the evolution of IF ridges and plateaus (Dorr, 1969). As shown in Fig. 4, caves are dominantly located at the scarp front and seldom extend



Fig. 23. Examples of canga/BIF transitions observed in caves. (A) Cave wall in Carajás displaying a later iron-rich sedimentary deposit of allochthonous origin (1) with some horizontal chemical Fe oxyhydroxide layers (2) overlying the folded weathered BIF (3). The original unlithified sediment was probably carried towards the cave and was indurated through Fe oxidation, resulting in "secondary" canga. (B) BIF bands in Carajás grading towards canga. The original banding structure, although fragmented, can still be recognized. This has been named as "structured canga" by Dorr (1964). (C) Sharp contact between BIF (below) and structured canga (top) in an IQ cave, with relict banding still preserved in the latter.

beyond it. They must evolve synchronously with the scarp retreat because otherwise they would have been removed from the landscape due to the dismantling and upslope migration of the scarp line. Caves tend to occupy over half of the vertical canga profile creating a mechanically unstable zone at the scarp front. Collapse leads to the generation of arcuate scarp lines, which will give rise to parallel (curved) vertical unloading joints that will further promote scarp dismantling. Through this positive feedback, coalescence and amplification of amphitheaters may lead to cusps (Fig. 5A), resulting in major asymmetrical indentations in ridges and plateaus. Such large cusps can exert control over the hydraulic gradient, forcing convergence of interflow lines and channeling sediment/solute delivery towards the lower and more pronounced cuspate scarp line.

IF landscapes are nearly always located at higher elevation and so there is no input of allogenic material. They are also mostly devoid of soil. Since there is no input of Fe from external sources and limited net iron loss takes place, the entire IF landscape is progressively leached of more mobile constituents, evolving towards an endpoint in which most silica will have been removed from the system, yielding the high grade porous ore characteristic of the IF regions of Brazil. Caves are thus biogeochemical outlets and act as major players in iron mobilization processes. Caves are also determinant in the geomorphic evolution

of IF ridges and plateaus. IF landscapes comprise a dynamic ecogeosystem that has been active for millions of years and evolves mostly through a complex interplay of biogeochemical processes at the subsurface.

8. Conclusions

Silica (and carbonate) leaching, iron mobilization/concentration, and porosity generation are closely associated processes in IF regions. Together, they play a major role as large scale and long term geomorphic agents, controlling the evolution and degradation of the ancient IF landscapes. The fresh BIF is seldom found in near surface environments, as silica/carbonate leaching and iron mobilization alters its chemical composition and texture. Hypogene processes that took place since the deposition of BIF in the Proterozoic are responsible for initial porosity generation, as more mobile elements are removed from the system. The resulting rock usually displays relict banding and variable degrees of cohesiveness. It is a productive aquifer and dewatering for deep open cast iron mines has always proved to be challenging. Supergene processes controlled by groundwater flow and further removal of constituents result in a dual porosity aquifer with major transmissive horizons controlled by fractures and relict banding.

The common interception of voids at depths of several hundreds of meters attests to the existence of early porosity in the deep phreatic zone.

The friable nature of the weathered BIF renders it highly susceptible to erosion if not for being capped by canga, the iron-rich supergene duricrust that protects the subjacent rock. Canga display high millimeter to centimeter scale porosity that allows for fast infiltration of meteoric water towards the contact with the less permeable weathered BIF.

Thousands of caves have been identified in the three major IF regions of Brazil: Carajás, Iron Quadrangle and Southern Espinhaço. They can occur in three different geological situations, entirely in canga or in weathered BIF, or along the contact between these two rock types. Caves at the contact tend to be the more welldeveloped. Caves are nearly always associated with the scarp lines of IF plateaus and ridges, seldom extending more than 100 m beyond it. Morphology of caves show a highly irregular combination of rooms and narrow passages, suggesting that they evolve through the coalescence of individual rooms. Microbial metabolism is an important controller of IF weathering and stability. Coupled Fe(III) reducing and Fe(II) oxidizing processes can lead to canga formation and enhance its stability, while Fe(III) reducing activities distal to the cave walls, in the sub-muros, lead to IF dissolution and cave formation. Caves persistence in the landscape is favored by the sub-muros-covering Fe(III) oxyhydroxides, in the same way as with canga, both internally due to vertically oriented iron infiltration routes, and at the surface.

The heterogeneous and porous canga layer is the result of complex and dynamic processes involving multiple chemical and biological interactions. Canga is a unique rock that exhibits self-healing characteristics and is formed continuously. The subsurface transformation of weathered BIF into canga occurs approximately in equilibrium with denudation at the surface, allowing for the long term resilience of IF ridges and plateaus.

The generation of caves and micro porosity is critical to the geochemical dynamics of IF regions. They are major players of long lasting leaching of more mobile constituents, yielding high grade iron deposits. The scarp front is the *locus* of both solute and sediment leaching, with caves acting as geochemical outlets. Caves also play a major role in scarp retreat, through collapse of cave passages creating indentations in the scarp line and gradually decreasing the total area of cangacapped surfaces.

The mobile character of iron allows for the possibility of rehabilitation of IF regions through canga restoration. This is of paramount importance as severe degradation is inherently associated with iron mining operations (Sonter et al., 2017). This represents an area of active research (Gagen et al., 2019b; Levett et al., 2021) that should provide further information on rates and processes of bacterially mediated iron cycling.

Approximately 50% of IF landscapes in IQ and 20% in Carajás have already been severely impacted (Salles et al., 2019; Souza-Filho et al., 2019). This represents an irreversible loss to a unique ecosystem that comprises several subterranean species adapted to subsurface canga habitat (Auler et al., 2019; Trevelin et al., 2019) as well as endemic metal tolerant plant species (Skirycz et al., 2014; Zappi et al., 2019). IF areas, among the oldest landforms of the planet (Vasconcelos et al., 2019), have remarkable geo and biodiversity value and should be the focus of increased conservation efforts. Caves represent the only geomorphic element that is intrinsically protected by the Brazilian constitution and as such, improving the knowledge about caves and their protection zone may be, at present, the most straightforward way towards the creation of conservation areas in canga. Understanding the important role of iron and silica mobilization is key to encourage further research and protection of a remarkable dynamic environment with few equivalents on Earth.

Declaration of competing interest

The authors declare that they have no known competing financial interests or personal relationships that could have appeared to influence the work reported in this paper.

Acknowledgements

This paper results from many years of research in most IF regions in Brazil. Sampling was performed through SISBIO permit 35992. Several mining companies supported our research along the years, especially Anglo American, Vale and Gerdau. We thank the help of the staff of Carste Ciência Ambiental during field work and data processing. Luciana Alt, Vitor Moura and Ataliba Coelho provided photographs. Dr. Renato Paes de Andrade (University of São Paulo) allowed the use of the permeameter. Insightful reviews by Jo De Waele and Carlos Spier improved the manuscript. This work was supported by funding from the National Science Foundation Geobiology and Low Temperature Geochemistry program (NSF# 1645180).

Appendix A. Supplementary data

Supplementary data to this article can be found online at https://doi.org/10.1016/j.geomorph.2021.108068.

References

- Abreu, S.S., Macambira, J.B., Cabral, E.S., 2016. Geologia e petrografia de formações ferríferas com ênfase na gênese de cavidades em Serra Norte, Carajás-PA. Espeleo-Tema 27, 33–44.
- Albuquerque, A.R.L., Angélica, R.S., Gonçalves, D.F., Paz, S.P.A., 2018. Phosphate speleothems in caves developed in iron ores and laterites of the Carajás Mineral Province (Brazil) and a new occurrence of spheniscidite. Int. J. Speleol. 47, 53–67. https://doi.org/10.5038/1827-806X.47.1.2135.
- Allaby, M., 2013. A Dictionary of Geology And Earth Sciences. Oxford University Press, Oxford.
- Allaire, S.E., Roullier, S., Cessna, A.J., 2009. Quantifying preferential flow in soils: a review of different techniques. J. Hydrol. 178, 179–204. https://doi.org/10.1016/j.jhydrol. 2009.08.013.
- Alvares, C.A., Stape, J.L., Sentelhas, P.C., Gonçalves, J.L.M., Sparovek, G., 2014. Köppen's climate classification map for Brazil. Meteorol. Z. 222, 711–728. https://doi.org/10.1127/0941-2948/2013/0507.
- Amorim, L.Q., Granchamp, C.A.P., Bertachini, A.C., 2001. Dewatering of iron ore mines and capability to predict environmental impacts the experience of MBR. Proceedings International Mine Water Association Symposium. Belo Horizonte . https://www.imwa.info/docs/imwa_2001/Dewateringoflron.pdf.
- ANM (Agência Nacional de Mineração), 2020. Anuário Mineral Brasileiro. Principais Substâncias Metálicas. (25 pp.)ANM, Brasília. https://www.gov.br/anm/pt-br/centrais-de-conteudo/publicacoes/serie-estatisticas-e-economia-mineral/anuario-mineral/anuario-mineral-brasileiro/amb_2020_ano_base_2019_revisada2_28_09. pdf. (Accessed 20 August 2021).
- Aubrecht, R., Lánczos, T., Gregor, M., Schlögl, J., Šmida, B., Liščák, P., Brewer-Carias, C., Vlček, L., 2011. Sandstone caves on Venezuelan tepuis: return to pseudokarst? Geomorphology 132, 351–365. https://doi.org/10.1016/j.geomorph.2011.05.023.
- Auler, A.S., 2016. Cave protection as a cave conservation tool in the environmentally sensitive Lagoa Santa Karst. Acta Carsologica 45, 131–145. https://doi.org/10.3986/ac.v45i2.4429.
- Auler, A.S., Sauro, F., 2019. Quartzite and quartz-sandstone caves of South America. In: White, W.B., Culver, D.C., Pipan, T. (Eds.), Encyclopedia of Caves. Academic Press, Cambridge, pp. 850–860.
- Auler, A.S., Parker, C.W., Barton, H.A., Soares, G.A., 2019. Iron formation caves: genesis and ecology. In: White, W.B., Culver, D.C., Pipan, T. (Eds.), Encyclopedia of Caves. Academic Press, Cambridge, pp. 559–566.
- Auler, A.S., Piló, L.B., 2015. Caves and mining in Brazil: the dilemma of cave preservation within a mining context. In: Andreo, B., Carrasco, F., Durán, J.J., Jiménez, P., LaMoreaux, P. (Eds.), Hydrogeological And Environmental Investigations in Karst Systems. Springer, Berlin, pp. 487–496.
- Auler, A.S., Piló, L.B., Parker, C.W., Senko, J.M., Sasowsky, I.D., Barton, H.A., 2014. Hypogene cave patterns in iron ore caves: convergence of forms or processes. In: Klimchouk, A., Sasowsky, I.D., Mylroie, J.E., Engel, S.A., Engel, A.S. (Eds.), Hypogene Cave Morphologies. Special Publication 18. Karst Waters Institute, Leesburg, pp. 15–19.
- Axelrod, J.M., Carron, M.K., Milton, C., Thayer, T.P., 1952. Phosphate mineralization at Bomi Hill and Bambuta, Liberia, West Africa. Am. Mineral. 37, 883–909.
- Babinski, M., Chemale Jr., F., van Schmus, W.R., 1995. The Pb/Pb age of the Minas Supergroup carbonate rocks, Quadrilátero Ferrífero,Brazil. Precambrian Res. 72, 235–245. https://doi.org/10.1016/0301-9268(94)00091-5.

Baumgartner, J., Faivre, D., 2015. Iron solubility, colloids and their impact on iron (oxyhyd)oxide formation from solution. Earth Sci. Rev. 150, 520–530. https://doi. org/10.1016/j.earscirev.2015.09.003.

- Bekker, A., Slack, J.F., Planawsky, N., Krapez, B., Hofmann, A., Konhauser, K.O., Rouxel, O.J., 2010. Iron Formation: the sedimentary product of a complex interplay among mantle, tectonic, oceanic, and biospheric processes. Econ. Geol. 105, 467–508. https://doi. org/10.2113/gsecongeo.105.3.467.
- Bertachini, A.C., Pereira, B.A., Bertachini, D.P., De Felippo, M.A., Beale, G., 2018. Hydrogeology of soft iron ores and associated rocks. In: Martin, D., Stacey, P. (Eds.), Guidelines for Open Pit Slope Design in Weak Rocks. CSIRO, Clayton, pp. 291–295.
- Bittencourt, J., Gomide, A., Carmo, F., Buchmann, F.S., 2015. Registro paleontológico em caverna desenvolvida em formações ferríferas na Serra do Gandarela. In: Ruchkys, U.A., Travassos, L.E.P., Rasteiro, M.A., Faria, L.E. (Eds.), Patrimônio Espeleológico em Rochas Ferruginosas. Sociedade Brasileira de Espeleológia, Campinas, pp. 192–209.
- Bowden, D.J., 1980. Sub-laterite cave systems and other pseudo-karst phenomena in the humid tropics: the example of the Kasewe Hills, Sierra Leone. Z. Geomorphol. 24, 77–90. https://doi.org/10.1127/zfg/24/1984/77.
- Brasil, 1988. Constituição da República Federativa do Brasil de 1988. Presidência da República. http://www.planalto.gov.br/ccivil_03/constituicao/constituicao.htm. (Accessed 20 August 2021).
- Brasil, 1990. Decreto Federal 99.556. Presidência da República. http://www.planalto.gov.br/ccivil_03/decreto/1990-1994/D99556.htm. (Accessed 20 August 2021).
- Bruthans, J., Soukup, J., Vaculikova, J., Filippi, M., Schweigstillova, J., Mayo, A.L., Masin, D., Kletetschka, C., Rihosek, J., 2014. Sandstone landforms shaped by negative feedback between stress and erosion. Nat. Geosci. 7, 597–601. https://doi.org/10.1038/ngeo2209.
- Calapa, K.A., Mulford, M.K., Rieman, T.D., Senko, J.M., Auler, A.S., Parker, C.W., Barton, H.A., 2021. Hydrologic alteration and enhanced microbial reductive dissolution of Fe(III) (hydr)oxides under flow conditions in Fe(III)-rich rocks: contribution to caveforming processes. Front. Microbiol. 12, 1932. https://doi.org/10.3389/fmicb.2021. 696534.
- Calux, A., Cassimiro, R., Salgado, A., 2019. Caves in iron formations in the Quadrilátero Ferrífero, Minas Gerais, southeastern Brazil: lithological, morphological and hydrological setting and speleogenesis. Z. Geomorphol. 62, 125–144. https://doi.org/10. 1127/zfg/2019/0475.
- Campana, B., Hughes, F.E., Burns, W.G., Whitcher, I.G., Muceniekos, E., 1964. Discovery of the Hamersley iron deposits. Proc. Aust. Inst. Min. Metall. 210, 1–30.
- CANIE (Cadastro Nacional de Informações Espeleológicas), 2021. https://www.icmbio. gov.br/cecav/canie.html.
- Carmo, F.F., Jacobi, C.M., 2016. Diversity and plant trait-soil relationships among rock outcrops in the Brazilian Atlantic rainforest. Plant Soil 403, 7–20. https://www.jstor.org/ stable/43872630.
- Carneiro, S.R.C., Marques, E.A.G., Chiste-Costa, J.P., 2016. Evaluation of hydraulic conductivity of itabirites of the Alegria Centro and Alegria Sul open pits, Samarco Mineração S.A., Minas Gerais state, Brazil. Mine Water Environ. 35, 136–144. https://doi.org/10.1007/e.10330.015.0328.6
- Carvalho, J.B., 2012. Avaliação isotópica e hidroquímica na porção noroeste do Aquífero Cauê, Quadrilátero Ferrífero, Brasil. Centro de Desenvolvimento da Tecnologia Nuclear, Belo Horizonte (MSc Dissertation).
- Chase, C.G., 1992. Fluvial landsculpting and the fractal dimension of topography. Geomorphology 5, 39–57. https://doi.org/10.1016/0169-555X(92)90057-U.
- Chiste-Costa, J.P., 2017. Numerical Groundwater Flow Modeling Applied to Dewatering Prediction of Cauê Aquifer in Alegria Mine, East of Quadrilátero Ferrífero, Minas Gerais. University of São Paulo, São Paulo (MSc Dissertation).
- Cornell, R.M., Schwertmann, U., 2003. The Iron Oxides: Structure, Properties, Reactions, Occurences And Uses. Wiley, Weinheim.
- Costa, T., Sá, G., 2018. Soft iron ores: geotechnical characteristics. In: Martin, D., Stacey, P. (Eds.), Guidelines for Open Pit Slope Design in Weak Rocks. CSIRO Publishing, Clayton South, pp. 273–285.
- CPRM, 2004. Projeto APA Sul RMBH: hidrogeologia, mapa hidrogeológico escala 1:50.000. SEMAD, CPRM, Belo Horizonte.
- Crundwell, F.K., 2017. On the mechanism of the dissolution of quartz and silica in aqueous solution. ACS Omega 2, 1116–1127. https://doi.org/10.1021/acsomega.7b00019.
- Curl, R.L., 1986. Fractal dimensions and geometries of caves. Math. Geol. 18, 765–783. https://doi.org/10.1007/BF00899743.
- Derby, O.A., 1910. The iron ores of Brazil. The Iron Ore Resources of the World. 2, pp. 813–822.
- Dias, J.C.S., Bacellar, L.A.P., 2021. A hydrogeological conceptual model for the groundwater dynamics in the ferricretes of Capão Xavier, Iron Quadrangle, Southeastern Brazil. Catena 207, 105633. https://doi.org/10.1016/j.catena.2021.105663.
- Dixey, F., 1920. Notes on laterization in Sierra Leone. Geol. Mag. 57, 211–220. https://doi.org/10.1017/S0016756800101530.
- Dorr, J.N., 1964. Supergene iron ores of Minas Gerais, Brazil. Econ. Geol. 59, 1203–1240. https://doi.org/10.2113/gsecongeo.59.7.1203.
- Dorr, J.N., 1965. Nature and origin of the high-grade hematite ore of Minas Gerais, Brazil. Econ. Geol. 60, 1–46. https://doi.org/10.2113/gsecongeo.60.1.1.
- Dorr, J.N., 1969. Physiographic. stratigraphic and structural development of the Quadrilátero Ferrífero, Minas Gerais, Brazil. U.S. Geological Survey Professional Paper 641-A.
- Dosseto, A., Turner, A., Chappell, J., 2008. The evolution of weathering profiles through time: new insights from uranum-series isotopes. Earth Planet. Sci. Lett. 274, 359–371. https://doi.org/10.1016/j.epsl.2008.07.050.
- Dosseto, A., Buss, H., Suresh, P.O., 2011. The delicate balance between soil production and erosion, and its role on landscape evolution. Appl. Geochem. 26, 524–527. https://doi. org/10.1016/j.apgeochem.2011.03.020.

Eschwege, W.L., 1822. Geognostisches Gemälde von Brasilien und wahrscheinliches Muttergestein der Diamanten. Landes-Industrie-Comptoir, Weimar.

- Ferreira, R.L., Oliveira, M.P.A., Silva, M.S., 2015. Biodiversidade subterrânea em geossistemas ferruginosos. In: Carmo, F.F., Kamino, L.H.Y. (Eds.), Geossistemas Ferruginosos Do Brasil. Instituto Prístino, Belo Horizonte, pp. 195–231.
- Figueira, R.L., Horbe, A.M.C., Aragón, F.F.H., 2019. Exotic sulfate and phosphate speleothems in caves from eastern Amazonia (Carajás. Brazil): crystallographical and chemical insights. J. S. Am. Earth Sci. 90, 412–422. https://doi.org/10.1016/j. isames.2018.12.007.
- Freeze, R.A., Cherry, J.A., 1979. Groundwater. Prentice Hall, Englewood Cliffs.
- Gagen, E.J., Levett, A., Shuster, J., Fortin, D., Vasconcelos, P.M., Southam, G., 2018. Microbial diversity in actively forming iron oxides from weathered banded iron formations systems. Microbes Environ. 33, 385–393. https://doi.org/10.1264/jsme2.ME18019.
- Gagen, E.J., Zaugg, J., Tyson, G., Southam, G., 2019a. Goethite reduction by a neutrophilic member of the alphaproteobacterial genus Telmanospirillum. Front. Microbiol. https://doi.org/10.3389/fmicb.2019.02938.
- Gagen, E.J., Levett, A., Paz, A., Gastauer, M., Caldeira, C.F., Valadares, R.B.S., Bitencourt, J.A.P., Alves, R., Oliveira, G., Siqueira, J.O., Vasconcelos, P.M., Southam, G., 2019b. Biogeochemical processes in canga ecosystems: armoring of iron ore against erosion and importance in iron duricrust restoration in Brazil. Ore Geol. Rev. 107, 573–586. https://doi.org/10.1016/j.oregeorev.2019.03.013.
- Gomes, M., Ferreira, R.L., Ruchkys, U.A., 2019. Landscape evolution in ferruginous geosystems of the Iron Quadrangle, Brazil: a speleological approach in a biodiversity hotspot. SN Appl. Sci. 1, 1102. https://doi.org/10.1007/s42452-019-1139-3.
- Gonçalves, J.A.C., Pereira, P.H.R., Vieira, E.M., 2018. Sistemas aquíferos: Hidrogeologia da porção nordeste do Quadrilátero Ferrífero na região de Itabira (MG). Proceedings XX Congresso Brasileiro de Águas Subterrâneas . https://aguassubterraneas.abas.org/asubterraneas/article/view/29349.
- Guedes, S.C., Rosière, C.A., Barley, M.E., 2013. The association of carbonate alteration of banded iron formation with the Carajás high-grade hematite deposits. Appl. Earth Sci. 112, 26–30. https://doi.org/10.1179/037174503225011234.
- Henwood, W.J., 1871. On the gold mines of Minas Geraes. Trans. R. Geol. Soc. Corn. 8, 168–370
- Jacobi, C.M., Carmo, F.F., Vincent, R.C., Stehmann, J.R., 2007. Plant communities in ironstone outcrops: a diverse and endangered Brazilian ecosystem. Biodivers. Conserv. 16, 2185–2200. https://doi.org/10.1007/s10531-007-9156-8.
- Jacobi, C.M., Carmo, F.F., Carmo, F.F., Campos, I.C., 2015. Iron geosystems: priority areas for conservation in Brazil. In: Tibbett, M. (Ed.), Mining in Ecologically Sensitive Landscapes. CSIRO Publishing, Clayton South, pp. 55–77.
- Jaffé, R., Prous, X., Zampaulo, R., Giannini, T.C., Imperatriz-Fonseca, L., Maurity, C., Oliveira, G., Brandi, I.V., Siqueira, J.O., 2016. Reconciling mining with the conservation of cave biodiversity: a quantitative baseline to help establish conservation priorities. Plos One 11 (12), 0168348. https://doi.org/10.1371/journal.pone.0168348.
- Jaffé, R., Prous, X., Calux, A., Gastauer, M., Nicacio, G., Zampaulo, R., Souza-Filho, P.W.M., Oliveira, G., Brandi, I.V., Siqueira, J.O., 2018. Conserving relicts from ancient underground worlds: assessing the influence of cave and landscape features on obligate iron cave dwellers from the Eastern Amazon. PeerJ 6, e4531. https://doi.org/10. 7717/peeri 4531
- Kambesis, P.N., Larson, E.B., Mylroie, J.E., 2016. Morphometric analysis of cave patterns using fractal indices. In: Feinberg, J., Gao, Y., Alexander, E.C. (Eds.), Caves And Karst Across Time. Geological Society of America Special Papers. 516, pp. 67–86. https:// doi.org/10.1130/2016.2516(06).
- Kinsella, A.S., Jones, A.M., Bligh, M.W., Pham, A.N., Collins, R.N., Harrison, J.J., Wilsher, K.L., Payne, T.E., Waite, T.D., 2016. Influence of dissolved silicate on rates of Fe(II) oxidation. Environ. Sci. Technol. 50, 11663–11671. https://doi.org/10.1021/acs.est. 6b03015
- Klein, C., 2005. Some Precambrian banded iron-formations (BIFs) from around the world: their age, geological setting, mineralogy, metamorphism, geochemistry, and origin. Am. Mineral. 90, 1473–1499. https://doi.org/10.2138/am.2005.1871.
- Klein, C., Ladeira, E.A., 2002. Petrography and geochemistry of the least altered banded iron formation of the Archean Carajás Formation, northern Brazil. Econ. Geol. 97, 643–651. https://doi.org/10.2113/gsecongeo.97.3.643.
- La Barbera, P., Rosso, R., 1989. On the fractal dimension of stream networks. Water Resour. Res. 25, 735–741. https://doi.org/10.1029/WR025i004p00735.
- Lagoeiro, L.E., 1998. Transformation of magnetite to hematite and its influence on the dissolution of iron oxide minerals. J. Metamorph. Geol. 16, 415–423. https://doi.org/10.1111/j.1525-1314.1998.00144.x.
- Laverty, M., 1987. Fractals in karst. Earth Surf. Process. Landf. 12, 475–480. https://doi.org/ 10.1002/esp.3290120505.
- Lemes, C.G.C., Villa, M.M., Felestrino, E.G., Perucci, L.O., Assis, R.A.B., Cordeiro, I.F., Fonseca, N.P., Guerra, L.C.C., Caneshi, W.L., Moraes, L.A.G., Carmo, F.F., Kamino, L.H.Y., Vale, P.N.C., Guima, S.E.S., Setubal, J.C., Salgado, A.R.R., Moreira, L.M., 2021. 16S rRNA gene amplicon sequencing data from the Iron Quadrangle ferruginous caves (Brazil) shows the importance of conserving this singular and threatened geosystem. Divers 13, 494. https://doi.org/10.3390/d13100494.
- Levett, A., Gagen, E., Shuster, J., Rintoul, L., Tobin, M., Vongsvivut, J., Bambery, K., Vasconcelos, P., Southam, G., 2016. Evidence of biogeochemical processes in iron duricrust formation. J. S. Am. Earth Sci. 71, 131–142. https://doi.org/10.1016/j.jsames. 2016.06.016.
- Levett, A., Gagen, E.J., Zhao, Y., Vasconcelos, P.M., Southam, G., 2020a. Biocement stabilization of an experimental-scale artificial slope and the reformation of iron-rich crusts. Proc. Natl. Acad. Sci. U. S. A. 117, 18347–18354. https://doi.org/10.1073/pnas. 2001740117.
- Levett, A., Vasconcelos, P.M., Gagen, E.J., Rintoul, L., Spier, C., Guagliardo, P., Southam, G., 2020b. Microbial weathering signatures in lateritic ferruginous duricrusts. Earth Planet. Sci. Lett. 538, 116209. https://doi.org/10.1016/j.epsl.2020.116209.

Levett, A., Gagen, E.J., Vasconcelos, P.M., Zhao, Y., Paz, A., Southam, G., 2020c. Biogeochemical cycling of iron: implications for biocementation and slope stabilization. Sci. Total Environ. 707, 136128, https://doi.org/10.1016/j.scitotenv.2019.136128.

- Levett, A., Gagen, E., Paz, A., Vasconcelos, P., Southam, G., 2021. Strategising the bioremediation of Brazilian iron ore mines. Crit. Rev. Environ. Sci. Technol. https://doi.org/10.1080/10643389.2021.1896346
- Liu, Y., Steenhuis, T.S., Parlange, J.Y., 1994. Formation and persistence of fingered flow in coarse grained soils under different moisture contents. J. Hydrol. 159, 187–195. https://doi.org/10.1016/0022-1694(94)90255-0.
- Lobato, L.M., Rosière, C.A., Silva, R.C.F., Zucchetti, M., Baars, F.J., Seoane, J.C.S., Rios, F.J., Pimentel, M., Mendes, G.E., Monteiro, A.M., 2005. A mineralização hidrotermal de ferro da Província Mineral de Carajás Controle estrutural e tectónico na evolução metalogenética da província. In: Marini, O.J., Queiroz, E.T., Ramos, B.W. (Eds.), Caracterização de Depósitos Minerais em Distritos Mineiros da Amazônia. ADIMB, Brasília, pp. 25–92.
- Lunevich, L., 2019. Aqueous silica and silica polymerization. In: Farahani, M.H.D.A., Vatanpour, V., Taheri, A.H. (Eds.), Desalination. Challenges And Opportunities. Intech Open, London https://doi.org/10.5772/intechopen.84824.
- Mandelbrot, B.B., 1977. Fractals: Form, Chance And Dimension. Freeman, San Francisco. Mandelbrot, B.B., 1983. The Fractal Geometry of Nature. Freeman, New York.
- Marescaux, M.G., 1973. Les grottes du Gabon Nord-oriental. Un "karst" dans l'oxyde de fer et la silice. Bull. Assoc. Géogr. Franç. 410, 607–618. https://doi.org/10.3406/bagf.1973. 4718.
- Maurity, C.W., Kotschoubey, B., 1995. Evolução recente da cobertura de alteração no Platô de N1 – Serra dos Carajás-PA. Degradação, pseudocarstificação, espeleotemas. Bol. Mus. Para. Emilio Goeldi. Série Ciências da Terra 7, 331–362.
- McFarlane, M., Twidale, C., 1987. Karstic features associated with tropical weathering profiles. Z. Geomorphol. (Suppl.64), 73–95.
- Mesquita, D.C., Dantas, J.C.M., Paula, R.S., Guerra, K.J., 2017. Estudo dos parâmetros hidrodinâmicos obtidos em ensaios de campo em itabiritos brandos da porção sudoeste do Quadrilátero Ferrífero, MG. Geonomos 25, 12–19. https://doi.org/10. 18285/geonomos.v25i2.1077.
- Monteiro, H.S., Vasconcelos, P.M., Farley, K.A., Spier, C.A., Mello, C.L., 2014. (U-Th)/He geochronology of goethite and the origin of Cangas. Geochim. Cosmochim. Acta 131, 267–289. https://doi.org/10.1016/j.gca.2014.01.036.
- Monteiro, H.S., Vasconcelos, P.M.P., Farley, K.A., 2018a. A combined (U-Th)/He and cosmogenic 3He record of landscape armoring by biogeochemical iron cycling. J. Geophys.Res. Earth Sci. 123, 298–323. https://doi.org/10.1002/2017JF004282.
- Monteiro, H.S., Vasconcelos, P.M.P., Farley, K.A., Lopes, C.A.M., 2018b. Age and evolution of diachronous erosion surfaces in the Amazon: combining (U-Th)/He and cosmogenic 3He records. Geochim. Cosmochim. Acta 229, 162–183. https://doi.org/10.1016/j.gca. 2018.02.045
- Morris, R.C., Fletcher, A.B., 1987. Increased solubility of quartz following ferrous-ferric iron reactions. Nature 330, 558–561. https://doi.org/10.1038/330558a0.
- Mourão, M.A.A., 2007. Caracterização hidrogeológica do Aquífero Cauê, Quadrilátero Ferrífero, MG. Universidade Federal de Minas Gerais, Belo Horizonte (DSc Thesis).
- Mota, N.F.O., Watanabe, M.T.C., Zappi, D.C., Hiura, A.L., Pallos, J., Viveros, A.M., Giuliétte, A.M., Viana, P.L., 2018. Amazon canga: the unique vegetation of Carajás revealed by the list of seed species. Rodriguésia 69, 1435–1488. https://doi.org/10.1590/2175-7860201869336.
- Nola, I.T.S., Bacellar, L.A.P., 2021. Multi-criteria analysis for mapping susceptibility to iron formation caves development in the Gandarela mountain range (MG), southeast Brazil. Int. J. Speleol. 50 (2), 173–187. https://doi.org/10.5038/1827-806X.50.2.2376.
- Palmer, A.N., 1991. Origin and morphology of limestone caves. Geol. Soc. Am. Bull. 103, 1–21. https://doi.org/10.1130/0016-7606(1991)103<0001:OAMOLC>2.3.CO;2.
- Palmer, A.N., 2007. Cave Geology. Cave Books, Dayton.
- Pardo-Igúzquiza, E., Dowd, P.A., Durán, J.J., Robledo-Ardila, P., 2018. A review of fractals in karst. Int. J. Speleol. 48, 11–20. https://doi.org/10.5038/1827-806X.48.1.2218.
- Parker, C.W., 2018. Microbial Iron Reduction in the Development of Iron Formation Caves. PhD DissertationUniversity of Akron, Akron.
- Parker, C.W., Auler, A.S., Senko, J.M., Sasowsky, I.D., Piló, L.B., Smith, M., Johnson, M., Barton, H.A., 2013a. Microbial iron cycling and biospeleogenesis: cave development in the Carajás Formation, Brazil. In: Filippi, M., Bosak, P. (Eds.), Proceedings of the 16th Congress of Speleology. 1. Czech Speleological Society, Prague, pp. 442–446.
- Parker, C.W., Wolf, J.A., Auler, A.S., Barton, H.A., Senko, J.M., 2013b. Microbial reducibility of Fe(III) phases associated with the genesis of iron ore caves in the Iron Quadrangle, Minas Gerais, Brazil. Minerals 3, 393–411. https://doi.org/10.3390/min3040395.
- Parker, C.W., Auler, A.S., Barton, M.D., Sasowsky, I.D., Senko, J.M., Barton, H.A., 2018. Fe(III) reducing microorganisms from iron ore caves demonstrate fermentative Fe(III) reduction and promote cave formation. Geomicrobiol J. 35, 311–322. https://doi.org/10.1080/01490451.2017.1368741.
- Paz, A., Gagen, E.J., Levett, A., Zhao, Y., Kopittke, P.M., Southam, G., 2020. Biogeochemical cycling of iron oxides in the rhizosphere of plants grown on ferruginous duricrust (canga). Sci. Total Environ. 713, 136637. https://doi.org/10.1016/j.scitotenv.2020. 136637.
- Piló, L.B., Auler, A.S., 2005. Cavernas em minério de ferro e canga de Capão Xavier. Quadrilátero Ferrífero,MG. O Carste 17, 92–105.
- Piló, L.B., Auler, A.S., Martins, F., 2015. Carajás National Forest: iron ore plateaus and caves in southeastern Amazon. In: Vieira, B.C., Salgado, A.A.R., Santos, L.J.C. (Eds.), Landscapes And Landforms of Brazil. Springer, Dordrecht, pp. 273–283.
- Pinheiro, R.V.L., 1997. Reactivation History of the Carajás And Cinzento Strike-slip System. Amazon. Brazil. University of Durham, Durham (PhD Thesis).
- Pissis, N.A., 1849. Mémoire sur la position géologique des terrains de la partie austral du Brésil et sur les soulèvements qui, à diverses époques, ont changé le relief de cette contrée. Mém. Inst. Fr. 10, 353–413.

Plotnick, R.E., Kenig, F., Scott, A., 2015. Using the voids to fill the gaps: caves, time and stratigraphy. In: Smith, D.G., Bailey, R.J., Burgess, P.M., Fraser, A.J. (Eds.), Strata And Time: Probing the Gaps in Our Understanding. 404. Geological Society, London, Special Publications. pp. 233–250.

- R Core Team., 2019. R: A Language And Environment for Statistical Computing. R Foundation for Statistical Computing, Vienna, Austria. https://www.R-project.org/.
- Reardon, E.J., 1979. Complexing of silica by iron(III) in natural waters. Chem. Geol. 25, 339–345. https://doi.org/10.1016/0009-2541(79)90066-4.
- Ribeiro, D.T., 2003. Enriquecimento supergênico de formações ferríferas bandadas: estruturas de colapso e desordem. Universidade Federal do Rio de Janeiro, Rio de Janeiro (DSc Thesis).
- Ribeiro, D., Moraes, I., Kwitko-Ribeiro, R., Braga, D., Spier, C., Santos, P., 2021. From fresh itabirites and carbonates to weathered iron ore: mineral composition, density and porosity of different fresh and altered rocks from the Quadrilátero Ferrífero,Brazil. Minerals 11, 29. https://doi.org/10.3390/min11010029.
- Rios, F.R., Santos Jr., A.E.A., 2015. Petrografia e caracterização de espeleotemas no testemunho de sondagem N4WS-1495 em formações ferríferas bandadas, Serra Norte, Província Mineral de Carajás. Proceedings 33° Congresso Brasileiro de Espeleologia, Sociedade Brasileira de Espeleologia, Eldorado, pp. 603–614.
- Rolim, V.K., Rosière, C.A., Santos, J.O.S., McNaughton, N.J., 2016. The Orosirian-Statherian banded iron formation-bearing sequences of the Southern border of the Espinhaço Range, Southeast Brazil. J. S. Am. Earth Sci. 65, 43–66. https://doi.org/10.1016/j.jsames.2015.11.003.
- Rosière, C.A., Heimann, A., Oyhantçabal, P., Santos, J.O.S., 2018. The iron formations of the South American Platform. In: Siegesmund, S., Basei, M.A.S., Oyhantçabal, P., Oriolo, S. (Eds.), Geology of Southwest Gondwana. Springer, Cham, pp. 493–526.
- Rosière, C., Spier, C.A., Rios, F.J., Suckau, V.E., 2008. The itabirites of the Quadrilátero Ferrífero and related high-grade iron ore deposits: an overview. In: Hagemann, S., Rosière, C.A., Gutzmer, J., Beukes, N.J. (Eds.), Banded Iron Formation-related Highgrade Iron Ore. Society of Economic Geologists, Littleton, pp. 223–254 https://doi.org/10.5382/Rev.15.09.
- Rosière, C., Stacey, P., 2018. Soft iron ores: geology. In: Martin, D., Stacey, P. (Eds.), Guidelines for Open Pit Slope Design in Weak Rocks. CSIRO Publishing, Clayton South, pp. 270–272.
- Ruchkys, U.A., Machado, M.M.M., 2013. Geological and mining heritage of Iron Quadrangle. Minas Gerais characterisation and strategies for education and geotourism. Bol. Parana. Geoci. 70, 120–136.
- Sagar, B.D., Chockalingam, L., 2004. Fractal dimension of non-network space of a catchment basin. Geophys. Res. Lett. 31. https://doi.org/10.1029/2004GL019749.
- Salgado, A., Braucher, R., Varajão, A.C., Colin, F., Varajão, A.F.D.C., Nalini Jr., H.A., 2008. Relief evolution of the Quadrilátero Ferrífero (Minas Gerais, Brazil) by means of (10Be) cosmogenic nuclei. Z. Geomorphol. 52, 317–323. https://doi.org/10.1127/0372-8854/2008.0052-0317.
- Salles, D.M., Carmo, F.F., Jacobi, C.M., 2019. Habitat loss challenges the conservation of endemic plants in mining-targeted Brazilian mountains. Environ. Conserv. 46, 140–146. https://doi.org/10.1017/S0376892918000401.
- Sasowsky, I.D., 2007. Clastic sediments in caves imperfect recorders of processes in karst. Acta Carsologica 36, 143–149. https://doi.org/10.3986/ac.v36i1.216.
- Sasowsky, I.D., Foos, A., Miller, C.M., 2000. Lithic controls on the removal of iron and remediation of acidic mine drainage. Water Res. 34, 2742–2746. https://doi.org/10.1016/S0043-1354(00)00019-1.
- Sauro, F., 2014. Structural and lithological guidance on speleogenesis in quartz–sandstone: evidence of the arenisation process. Geomorphology 226, 106–123. https://doi.org/10.1016/j.geomorph.2014.07.033.
- Sauro, F., De Waele, J., Onac, B.O., Galli, E., Dublyansky, Y., Baldoni, E., Sanna, L., 2014. Hypogenic speleogenesis in quartzite: the case of Corona 'e Sa Craba Cave (SW Sardinia, Italy). Geomorphology 211, 77–88. https://doi.org/10.1016/j.geomorph.2013. 12.031
- Schaefer, C.E.G.R., Corrêa, G.R., Candido, H.G., Arruda, D.M., Nunes, J.A., Araújo, R.W., Rodrigues, P.M.S., Fernandes Filho, E.I., Pereira, A.F.S., Brandão, P.C., Neri, A.V., 2016. The physical environment of rupestrian grasslands (campos rupestres) in Brazil: geological, geomorphological and pedological characteristics and interplays. In: Fernandes, G.W. (Ed.), Ecology And Conservation of Mountaintop Grasslands in Brazil. Springer, pp. 15–53.
- Scherer, R.S., 2017. Ocorrência de espeleotemas fosfáticos e feições morfológicas raras em cavernas ferríferas da Serra de Carajás no Pará. Instituto Tecnológico Vale, Belém.
- Silva Junior, R.O., Queiroz, J.C.B., Ferreira, D.B.S., Lima, A.T., Souza Filho, P.W.M., Guimarães, J.T.F., Rocha, E.P., 2017. Estimativa de precipitação e vazões médias Para a bacia hidrográfica do rio Itacaiúnas (BHRI). Amazônia Oriental, Brasil. Rev. Bras. Geogr. Fis. 10, 1638–1654. https://doi.org/10.26848/rbgf.v.10.5.p1638-1654.
- Silva, M.S., Martins, R.P., Ferreira, R.L., 2011. Cave lithology determining the structure of the invertebrate communities in the Brazilian Atlantic Rain Forest. Biodiver. Conserv. 20, 1713–1729. https://doi.org/10.1007/s10531-011-0057-5.
- Simmons, G.C., 1960. Origin of certain cangas of the "Quadrilátero Ferrífero" of Minas Gerais, Brazil. Bol. Soc. Bras. Geol. 9, 37–59.
- Simmons, G.C., 1963. Canga caves in the Quadrilátero Ferrífero, Minas Gerais, Brazil. Bull. Nat. Speleol. Soc. 25, 66–72.
- Simmons, G.C., 1964. Leucophosphite, a new occurrence in the Quadrilátero Ferrífero, Minas Gerais, Brazil. Am. Mineral. 49, 377–386.
- Skirycz, A., Castilho, A., Chaparro, C., Carvalho, N., Tzotzos, G., Siqueira, J.O., 2014. Canga biodiversity, a matter of mining. Front. Plant Sci. 5, 653. https://doi.org/10.3389/ fpls 2014 00653
- Sonter, L.J., Herrera, D., Barrett, D.J., Galford, G.L., Moran, C.J., Soares-Filho, B.S., 2017. Mining drives extensive deforestation in the Brazilian Amazon. Nat. Comm. 8, 1013. https://doi.org/10.1038/s41467-017-00557-w.

Souza-Filho, P.W., Giannini, T.C., Jaffé, R., Giulietti, A.M., Santos, D.C., Nascimento Jr., W.R., Guimarães, J.T.F., Costa, M.F., Imperatriz-Fonseca, V.L., Siqueira, J.O., 2019. Mapping and quantification of ferruginous outcrop savannas in the Brazilian Amazon: a challenge for biodiversity conservation. Plos One 14 (1), e0211095. https://doi.org/10. 1371/journal.pone.0211095.

- Spier, C.A., Levett, A., Rosière, C.A., 2019. Geochemistry of canga (ferricrete) and evolution of the weathering profile developed on itabirite and iron ore in the Quadrilátero Ferrífero, Minas Gerais, Brazil. Miner. Depos. 54, 983–1010. https://doi.org/10.1007/ s00126-018-0856-7.
- Spier, C.A., Oliveira, S.M.B., Rosière, C.A., 2003. Geology and geochemistry of the Águas Claras and Pico iron mines, Quadrilátero Ferrífero, Minas Gerais, Brazil. Miner. Depos. 38, 751–774. https://doi.org/10.1007/s00126-003-0371-2.
- Spier, C.A., Oliveira, S.M.B., Sial, A.N., Rios, F.J., 2007. Geochemistry and genesis of the banded iron formations of the Cauê Formation, Quadrilátero Ferrifero, Minas Gerais, Brazil. Precambrian Res. 152, 170–206. https://doi.org/10.1016/j.precamres.2006.10. 003
- Spier, C.A., Vasconcelos, P.M., Oliveira, S.M.B., 2006. 40Ar/39Ar geochronological constraints on the evolution of lateritic iron deposits in the Quadrilátero Ferrífero, Minas Gerais, Brazil. Chem. Geol. 234, 79–104. https://doi.org/10.1016/j.chemgeo. 2006 04 006
- Suchý, V., Sýborová, I., Zachariáš, J., Filip, J., Machovič, V., Lapčák, L., 2017. Hypogene features in sandstone: an example from Carboniferous basins of Central and Western Bohemia, Czech Republic. In: Klimchouk, A., Palmer, A.N., De Waele, J., Auler, A.S., Audra, P. (Eds.), Hypogene Karst Regions And Caves of the World. Springer, Cham, pp. 313–328.
- Trendall, A.F., Basei, M.A.S., de Laeter, J.R., Nelson, D.R., 1998. SHRIMP zircon U-Pb constraints on the age of the Carajás formation, Grão Pará Group, Amazon Craton. J. S. Am. Earth Sci. 11, 265–277. https://doi.org/10.1016/S0895-9811(98)00015-7.

- Trevelin, L.C., Gastauer, M., Prous, X., Nicácio, G., Zampaulo, R., Brandi, I., Oliveira, G., Siqueira, J.O., Jaffé, R., 2019. Biodiversity surrogates in Amazonian iron cave ecosystems. Ecol. Indic. 101, 813–820. https://doi.org/10.1016/j.ecolind.2019.01.
- Twidale, C.R., Horwitz, R.C., Campbell, E.M., 1985. Hamersley landscapes of Western Australia. Ver. Géol. Dynam. Géogr. Phys. 26, 173–186.
- Vasconcelos, P.M., Carmo, I.O., 2018. Calibrating denudation chronology through 40Ar/ 39Ar weathering geochronology. Earth Sci. Rev. 179, 411–435. https://doi.org/10. 1016/j.earscirev.2018.01.003.
- Vasconcelos, P.M., Farley, K.A., Stone, J., Piacentini, T., Fifield, L.K., 2019. Stranded land-scapes in the humid tropics: Earth's oldest land surfaces. Earth Planet. Sci. Lett. 519, 152–164. https://doi.org/10.1016/j.epsl.2019.04.014.
- Wang, Y., Li, Y., Wang, X., Chau, H.W., 2018. Finger flow development in layered water-repellent soils. Vadose Zone J. 17, 170171. https://doi.org/10.2136/vzj2017.09.0171.
- Weber, K.A., Achenbach, L.A., Coates, J.D., 2006. Microorganisms pumping iron: anaerobic microbial iron oxidation and reduction. Nat. Rev. Microbiol. 4, 752–764. https://doi. org/10.1038/nrmicro1490
- Wray, R.A., Sauro, F., 2017. An updated global review of solutional weathering processes and forms in quartz sandstone and quartzites. Earth Sci. Rev. 171, 520–557. https:// doi.org/10.1016/j.earscirev.2017.06.008.
- Zappi, D.C., Moro, M.F., Walker, B., Meagher, T., Viana, P.L., Mota, N.F.O., Watanabe, M.T.C., Lughadha, E.N., 2019. Plotting a future for Amazonian canga vegetation in a campo rupestre context. Plos One 14 (8), e0219753. https://doi.org/10.1371/journal.pone. 0219753.